WISC

UC-20 f

UNIVERSITY OF WISCONSIN • MADISON, WISCONSIN

PLASMA PHYSICS

MEASUREMENT OF CONVECTIVE CELL SPECTRA AND THE RESULTANT CALCULATED VORTEX DIFFUSION COEFFICIENT

A. Butcher Ehrhardt[+] and R.S. Post

DOE/ET53051/12

October 1980

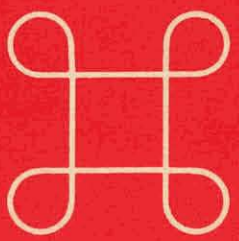

ONSIN

DISCLAIMER

NOTICE

Printed in the United States of America
Available from
National Technical Information Service
U.S. Department of Commerce
5285 Port Royal Road
Springfield, VA 22161

NTIS Price codes
Printed copy: A03
Microfiche copy: A01

MEASUREMENT OF CONVECTIVE CELL SPECTRA AND THE RESULTANT CALCULATED VORTEX DIFFUSION COEFFICIENT

A. Butcher Ehrhardt[+] and R.S. Post

University of Wisconsin, Madison, Wisconsin, 53706, U.S.A.

ABSTRACT

The presence of convective cells in a purely poloidal field Levitated Octupole has been associated with diffusion that scales as $D_v \propto (T^*/n)^{1/2}$, independent of B, where T* is an "effective temperature," $T^* \propto T$.

The electric field spectrum of the convective cells can be used to estimate the magnitude of T* and D_v. The results are in reasonable agreement with previous measurements of cross-field transport, and agree qualitatively with theoretical models of vortex diffusion.

[+]Current address: Johns Hopkins University, Applied Physics Laboratory, Laurel, MD, 20810.

I. INTRODUCTION

Floating potential structure has been measured in many experimental plasma devices[1-4]. In the Wisconsin Levitated Octupole a correlation was noted between the presence or absence of these convective cells or vortices and the type of diffusion needed to explain particle losses[5]. In the parameter regimes where classical diffusion was measured there was little potential structure. In the parameter regimes where use of a vortex diffusion coefficient correctly predicted the scaling of the diffusion with density and magnetic field strength, machine-sized potential cells were measured ($\phi \sim 0.3$ KT/e).

We are interested in comparing convective cells and spectra in a collisional[5] ($\lambda_{mfp} << L_c$) and a collisionless[6] ($\lambda_{mfp} >> L_c$) plasma with observed diffusion (λ_{mfp} is the particle mean free path and L_c is the connection length). The profile evolution studies[5,6] of diffusion in the Octupole with a purely poloidal field can all be explained within the framework of vortex diffusion:

$$D_v \propto \frac{1}{B}\sqrt{\frac{T}{\varepsilon}} \quad , \quad \varepsilon = 1 + \frac{\omega_{pi}^2}{\omega_{ci}^2} \, , \tag{1}$$

noting that classical collisional viscosity and diffusion are always present, and will dominate the transport at sufficiently low fields for a collisional plasma.

The collisional plasma exhibits classical diffusion ($D_{cl}=D_o n/B^2$) at low fields ($B \lesssim 100G$). As B is increased, there is a transition to vortex diffusion scaling with $\varepsilon >> 1$. D is proportional to $(T^*/n)^{1/2}$ and independent of B, and the magnitude of D indicates an "effective temperature"[5] T^* of 10^6 eV. At high fields, with $\varepsilon >> 1$, the transport in the collisionless plasma is

dominated by vortex diffusion with $T^* \simeq 10^4$ eV [6]. As predicted by equation (1), the scaling becomes independent of density, and is proportional to B^{-1}, as the density is reduced to the point where the dielectric coefficient approaches unity.

Recent theoretical work has been done on two-dimensional plasmas. The importance of the theory for the Octupole lies in that, with a few modifications and extensions, 2-D fluid theory can be used to predict both vortex diffusion and macroscopic vortex structure, remarkably like that observed in the Octupole. J. B. Taylor[7] has shown that 3-D systems have contributions to diffusion from both vortex modes and from collisions. The vortex contribution will dominate if there is sufficient energy in the $k_{||}=0$ modes. With a purely poloidal field the potential is constant along a field line[8], all of the vortex energy is in the $k_{||}=0$ modes, and we will expect to see vortex diffusion except for very dense, cold plasmas in low magnetic fields, or for plasmas where the vortex spectrum has damped away.

We have studied the plasma regimes where the diffusion scales like vortex diffusion, $D_v \propto (T^*/n)^{1/2}$, $T^* \propto T_e$, and independent of B. The vortex diffusion coefficient can be derived in several ways. Okuda and Dawson[9] calculated the diffusion coefficient for a 2-D thermal plasma from the linearized two-fluid equations to obtain

$$D_v \propto \sqrt{\frac{T}{n}} \quad , \quad \text{independent of B.} \tag{2}$$

Taylor and McNamara[10] investigated the 2-D electrostatic guiding-center plasma and found D for an arbitrary electric field spectrum,

$$D = \frac{1}{B}\sqrt{\Sigma \frac{E^2(k)}{k^2}} \tag{3}$$

In thermal equilibrium the energy per k-mode is T/2. Okuda and Dawson have shown that a fraction $1/\varepsilon$ of this energy is associated with the low frequency vortex modes. The electric field energy in the vortex modes is thus $(\varepsilon E^2_k/8\pi)\cdot \ell_\perp^2 \ell_{||}$, where $\ell_{||}$ and $\ell_\perp$ are the lengths parallel and transverse to the field lines[6]. For a non-thermal plasma we can define an effective temperature T^* analogously as

$$\frac{T^*(k)}{2} = \frac{\varepsilon E^2(k)}{8\pi} \ell_\perp^2 \ell_{||} \tag{4}$$

and estimate the value of T^* by measuring $E^2(k)$, n, and B.

The Okuda-Dawson diffusion coefficient predicts the correct scaling for the diffusion but is too small to explain the observed diffusion in the Octupole by several orders of magnitude if the thermodynamic temperature is used. The effective temperatures calculated from the toroidal electric field spectra presented in this paper are much larger than the thermodynamic temperatures, and are large enough to account for the observed vortex diffusion.

II. CALCULATION OF A DIFFUSION COEFFICIENT

Taylor and McNamara[10] calculated the diffusion coefficient for the guiding-center plasma. Diffusion comes about when the electric fields in the plasma become uncorrelated; in an equilibrium plasma this is due to statistical fluctuations about the ensemble average. The expression obtained by Taylor and McNamara is

$$\overleftrightarrow{D}(t) = \frac{d\overleftrightarrow{R}}{dt} = \frac{1}{2B}\sqrt{\sum_k \langle E^2(k)\rangle[1 - e^{-2k^2 R}]} \qquad (5)$$

where R(t) is the mean dispersion of a group of diffusing particles. For very long times R(t) is unbounded, and D is given by equation (3).

Equation (5) is a tensor equation, representing four separate equations coupled by the exponential term. To solve this equation completely we need to expand the electric field in eigenfunctions suitable for the Octupole, and then solve the four coupled equations simultaneously. The Octupole coordinates perpendicular to B are ψ and θ. Eigenfunctions in these coordinates can be found by considering Poisson's equation. Using the differential operators in the appendix, it can be shown that Poisson's equation is separable in Octupole coordinates. The eigenfunctions in θ are the toroidal eigenfunctions, $e^{ik\theta}$; the potential structure can be Fourier-transformed in θ to obtain the amplitudes of the toroidal modes.

We are interested in the net diffusion across a ψ-surface (the net diffusion in θ is zero), so we need only the solutions to the equations for $d^2R_{\psi\psi}/dt^2$ and $d^2R_{\psi\theta}/dt^2$. The exponential in (5), in Octupole coordinates, is

$$\exp\,[-2\,(k_\psi^2\,R_{\theta\theta} - k_\psi k_\theta(R_{\psi\theta} + R_{\theta\psi}) + k_\theta^2\,R_{\psi\psi})]$$

The first assumption we will make is that $D_{\psi\psi} >> D_{\psi\theta}$. The second assumption is that the exponential is dominated by the term $k^2_\theta R_{\psi\psi}$. These assumptions imply that the diffusion is caused by the energy in the azimuthal electric fields. Not enough is known about the $\langle E_\psi E_\theta\rangle$ amd $\langle E_\psi E_\psi\rangle$ correlations yet to prove definitely that this ordering is correct because of the lack of spatial

resolution with the cart probe (see Section III); however, there should be no diffusion across a ψ-surface due to vortex modes unless there are azimuthal potential gradients.

With these assumptions, equation (5) reduces to

$$\frac{d^2 R_{\psi\psi}}{dt^2} = \frac{1}{2B^2} \sum_k \langle E_\theta^2(k) \rangle \exp\left(-2k_\theta^2 R_{\psi\psi}\right) \tag{6}$$

This equation is very similar to Taylor and McNamara's expression for d^2R/dt^2 (Ref. 10), with the exception that it emphasizes that the toroidal spectrum and eigenmodes should be used to determine diffusion ($D=dR_{\psi\psi}/dt$) in the ψ direction. To estimate the net diffusion across a ψ-surface we integrate (6) on the closed flux surface. Substituting the expressions for ϕ, E_θ, and v_ψ in Octupole coordinates given in the appendix into the equation for D we obtain

$$D = \frac{R}{B}\left[\sum_k \frac{E^2(k)}{k^2}\right]^{1/2}$$

Averaging the flux over a ψ-surface, we can define $\mathcal{D}(\psi)$,

$$\Gamma_{av} = \frac{\int D \cdot \nabla n \, dA}{dA} = \frac{\int D \, \nabla n \, R \, d\theta d\ell}{\int R \, d\theta d\ell}$$

$$= \left[\sum_k \langle \phi(k)^2 \rangle\right]^{1/2} \cdot 2\pi \frac{\int R^2 d\theta d\ell}{\int R d\ell} \cdot \frac{\partial n}{\partial \psi} = F(\psi) \cdot G(\psi) \cdot \frac{\partial n}{\partial \psi}$$

$$= \mathcal{D}(\psi) \cdot \frac{\partial n}{\partial \psi} \tag{7}$$

$\mathcal{D}(\psi)$ consists of a function $F(\psi)$ which is independent of θ, and a geometrical factor $G(\psi)$[11]. To put the diffusion coefficient in units appropriate to compare with Γ, we multiply $\partial n/\partial \phi$ by the average value of $2\pi RB$ over the ψ-surface.

$$\Gamma_{av} = \frac{\mathcal{D}(\psi)}{2\pi RB}_{av} \cdot \nabla n = \mathcal{D}_{av} \cdot \nabla n \qquad (8)$$

To use this equation we need the correlation of the velocity field over an ensemble; it is especially important if the number of 'most probable states' is large--and they are substantially different. This is the case if the energy is concentrated in small vortices which fit into the 'box' in many ways. However, when the most probable states are few or indistinguishable (as in the case where the structure tends towards a large vortex, or pair of vortices, which can fit in the box in only one or two ways), the most probable state should be the same as the actual state of the system. The observed vortex structure in the Octupole corresponds to the latter case--the shorter wavelength cells have small amplitudes, and the structure of the large vortices is reproducible. Therefore, the assumption is made that the reproducible structure measured in the Octupole represents the most probable state, and that the ensemble average can be replaced by the measured spectra.

The differential equation was solved numerically using a predictor-corrector algorithm, with an approximation for small k^2R to start the solution. Because the spectrum is peaked at the lowest mode, it was not found necessary to include modes higher than k=30 in the solution.

The dielectric coefficient depends on n/B^2 for $\omega_{pi}^2/\omega_{ci}^2 > 1$, and is large near the density peak relative to its value near the Octupole walls. If $T^* \propto \varepsilon E^2$ is a constant in the plasma as the transport studies[6] suggest, then we expect the electric field spectrum to vary in ψ, as is observed.

III. EXPERIMENTAL APPARATUS

The Wisconsin Levitated Octupole has been extensively described elsewhere[12-15]. It is a pulsed machine; the four internal hoops are the

secondary of a 90-to-1 transformer. The magnetic field lines are shown in Fig. 1. The average magnetic field in the private flux, B_{ave}, is defined[6] as one-half of the average field strength on the surface of the large major radius ring; the average field strength for the inner hoops is roughly twice as large as the value for the outer hoops.

Data to be presented was all taken with the field crowbarred at 25 msec, slightly after peak field. The L/R decay time for the magnetic field varies from ~ 95 msec near the rings to ~ 165 msec near the center of the machine[16]. This allows experiments to be done in a slowly-varying magnetic field. A high current SCR and solid state diode[17] allow operation with a crowbarred field even at very low bank voltages.

The potential depends only on θ (azimuthal angle) and ψ (flux surface). Therefore, to obtain a 3-D picture of the floating potential structure, ϕ is measured at one position on each field line as a function of θ. Dr. J.R. Drake[12] designed a cart with a movable probe to measure $\phi(\psi,\theta)$. The cart was mounted on rails on the bottom lid, at a radius slightly greater than the lower inner hoop (at R~1.1m). The cart could be moved through an azimuthal angle of 350°, from -90°, past the gap (at 0°), through 240°. The cart was insulated from the rails and the machine by Teflon wheels, and carried miniature coaxial cables for signals from up to four Langmuir probes. The probes' frequency response was limited to $\lesssim$ 1 kHz by the cable capacitance.

As shown in Fig. 1, the probe can be rotated through an angle α of approximately 100° so as to sweep through portions of the lower lid mid-cylinder side of the private flux of both lower hoops. The probe has the general shape indicated in Fig. 1, with a shallow bend in the middle. This enables access quite close to the inner wall and inner ring (position A), and allows the probe to avoid hitting the microwave mirrors, etc., on the

lower lid (position B). The probe tips were 2 mm and 3 mm gold balls mounted on 1/32" ceramic stalks; the probe body is of 1/8" ceramic. The probes had either 1 or 2 tips at the bend and 2 tips at the end.

The Octupole was operated on a 1-1/2 minute cycle; during this time the experimenter could examine the digitized signals from the cart and monitor probes, and a "movie" showing $\phi(\theta)$ for the current ψ-surface scan. Floating potential contours were plotted by repeating this procedure for several values of ψ to construct a 2-D grid. Typically 4 to 6 psi-surfaces per tip were scanned; the grid step size in θ varied from about .4° to 6° depending on the experiment[8].

Fig. 7 shows typical cell plots. The magnetic field will be normal to the plots, and for a given plot will be either into, or out of, the page, but not both. The physical dimensions for the full range of values in ψ(0-10 Dories) are on the order of 10-50 cm, and for 360° in θ, $2\pi R \sim 2\pi(1.4\ m) \sim 9$ m. If the plots were done in real space they would be sectors of a thin annulus, and if shown more nearly to scale, the contour plots would be long and thin.

A fixed Langmuir probe was used to monitor the reproducibility of the gun plasmas. The changes in V_f for a fixed position of the cart probe did not correlate with changes in V_f at the monitor probe, making it impossible to normalize the data using the monitor probe. Instead a norm was defined as the area under the curve for the monitor signal, and an accepance criterion was defined about the norm--shots in which the monitor was outside of this percentage were rejected. The acceptance range was 10% about the norm for the high density plasma (this plasma tends to be very reproducible--most shots fell within 5%), and 15% for the low density plasma. Gun plasmas in the Octupole have uniform temperatures[14,17]; therefore floating potential contours have been used to infer the electric fields in the plasma.

IV. EXPERIMENTAL OBSERVATIONS

Collisional Plasma.

An experiment performed with the collisional plasma in which contours were plotted for a range of magnetic field strengths was reported in Ref. 5. The results of that experiment can be summarized as follows: at high fields (B_{ave}~800 G), where $D_v > D_{cl}$, macroscopic vortices were present, and did not damp away during the experimental period. In the transition regime (B_{ave}~300 G) vortices were observed to damp on an ion viscous damping time scale. At very low fields (B_{ave}~180 G) the cell structure is much smaller than at high fields by the earliest time observed (7 msec after injection) due to a shorter viscous damping time.

In a second experiment with the collisional plasma the toroidal spectrum of $\phi(k)$ was measured for a single ψ-surface (ψ=3.4) in the private flux of the lower outer hoop. Fig. 2 shows $\phi(k)$ vs k for B_{ave}~600 G, and Fig. 3 shows $\phi(k)$ for B_{ave}~180 G. The spectra are plotted at 2 msec, 10 msec, and 20 msec after injection. Both show that $\phi(k)$ is a decreasing function of k; the electric field spectrum for the low-field case drops off faster with increasing k than the high-field case.

$\mathcal{D}(\psi,t)$ obtained from $\phi(k)$ and eq. 7 is plotted in Figs. 4 and 5 for the two cases. The electric field spectrum is smaller in amplitude for the low-field case (Fig. 6); however, $\mathcal{D}(\psi)$ obtained is an order of magnitude larger. We can calculate D_{cl} for both cases[17], using

$$D_{cl} = 1.65 \times 10^{-4}\ \mathrm{cm^5 eV^{1/2} G^2 sec^{-1}}\ \frac{n}{B^2 T_e^{1/2}}$$

With $n \sim 2 \times 10^{\pm 11}$, $T_e \sim 0.2$ eV, we find D_{cl} (B_{ave}~600 G) = 200 cm^2/sec for the high field-case, and for the low-field case, D_{cl} = 1200 cm^2/sec. The ratio

D_v/D_{cl} is ~ 25 for the high field case. For the lower field case this ratio is reduced (to ~ 8). The ratio $D_v/D_{cl} \sim 1$ occurs at about 100 G for this plasma[5]. Taking into account that D_v calculated from the electric field spectrum is a rough estimate which tends to be somewhat higher than the values calculated by profile matching, the data presented here is consistent with the data in Ref. 5.

In a third experiment with the collisional plasma a 360° scan of six ψ-surfaces in the private flux of the lower inner hoop was made with B_{ave}~240 G. The contour plots are shown in Fig. 7. The cell pattern is very clear. There are two large cells: a positive cell centered at ψ = 2.75, θ = 250°, and a negative cell centered at ψ = 4.5, θ = 70°, halfway around the machine in θ from the positive cell. The cell structure does not lose its identity in the 70 msec observation period, although it decays in amplitude by about a factor of 2 over the same period.

The power spectrum for the six ψ-surfaces, $E_\theta^2(k)$, is shown in Fig. 8a-f (3 msec after injection) and Fig. 9a-f (7 msec). The plots show that E^2 is a decreasing function of k. The E^2 power spectrum is a strong function of position in ψ. The separatrix has little structure; the amplitude of the structure increases towards the ring. $\Sigma E^2(k)$ is plotted in Fig. 10 for the six ψ-surfaces measured, at 4 times. The earliest time plotted is 10 msec after injection (at earlier times the structure is not reproducible). We have used the E^2 data to estimate the diffusion coefficient for this plasma as a function of ψ-surface and time. The results are presented in Fig. 11. Because of the ψ-dependence of E^2, the diffusion coefficient is also ψ-dependent, with the separatrix region having the smallest values of D_v. The diffusion increases during the first 5-10 msec and then becomes constant, except for the two ψ-surfaces closest to the ring. D_v is lowest near the separatrix, where it has a value ~ 500 cm^2/sec. The magnitude of D_v for this

plasma is in reasonable agreement with the results shown in Ref. 5, and the shape of $D_v(\psi)$ is roughly what would be expected for $D_v \propto n^{-1/2}$ (see, for example, Ref. 14, Fig. 3.21).

We can estimate T*(k) from equation (4) using $n \sim 10^{11}/cm^3$, B = 240G × 2 (for the inner hoop), and E(k=1) = .02 V/m, which leads to $T^*(k=1) = 5.6 \times 10^7$ eV. This is consistent with the average $T^* \sim 10^6$ eV quoted in Ref. 5 for a T* independent of k.

Collisionless Plasma.

The floating potential contours for a 360° scan of the lower inner hoop are given in Fig. 12a-d (private flux). This data shows the characteristic cell pattern for a collisionless plasma with the machine supported: the three inner supports are clearly visible in the private flux contours. The cell structure is stationary in space; although the field lines are soaking into the rings and walls, the cells do not move with them.

The toroidal spectrum of the electric field is shown in Figs. 13 and 14 for two psi-surfaces in the private flux of the lower inner hoop (ψ=4.09 and 4.52). The figures show that the energy spectrum of the toroidal vortex modes is a rapidly decreasing function of k, and decays in time. The toroidal spectrum (Figs. 13 and 14) is enhanced in amplitude over a thermal spectrum, and has the shape of an inverse cascade in contrast to a thermal spectrum which is flat from $k = \frac{1}{L}$ to $k = \frac{1}{\lambda}$.

The value of the diffusion coefficient $D_v(t)$ calculated from the spectra in Figs. 13 and 14 for the two ψ-surfaces in the LIH private flux is plotted in Fig. 15. The computed D_v is on the order of 10^4 cm^2/sec 5 msec after injection, decreases to $\sim 2.5\text{-}3.5 \times 10^3$ cm^2/sec by 20 msec, and then levels off, and begins to climb very slowly. The behavior of D(t) agrees in general with

the profile evolution results[6]: initially, T* decays rapidly, and because $D \propto (T^*/n)^{1/2}$, D will also decrease; after 30 msec, T* is constant, but n is still decaying, so that D will increase in time. The magnitude of D_v calculated from the spectra after 20 msec is larger by a factor of 2-5 than the 800 cm^2/sec quoted in Ref. 6, Fig. 2. This is remarkably good agreement considering that our results are from a relatively crude calculation made on limited data.

The enhanced temperature T* can be estimated from equation (4) using the value of $E^2(k=1) = .075\ V^2/m^2$ at 25 msec from Fig. 13 (ψ=4.1); with $n \simeq 2 \times 10^7/cm^3$, B ~ 2 kG, $V = 8 \times 10^4\ cm^3$, we find $T^*(k=1) = 2.4 \times 10^5$ eV. This estimate is very rough, but it shows that there is enough energy in the vortex spectrum to account for the observed diffusion.

V. DISCUSSION

The contour plots and spectra are similar to those obtained in numerical simulations of the guiding center plasma[18]. The equations of motion of the 2-D electrostatic guiding-center plasma are formally identical to the equations of motion for 2-D inviscid Navier-Stokes fluid turbulence if the charge density ρ is identified with the vorticity Γ; potential contours correspond to streamlines. In this model energy and vorticity are conserved, and the non-linear interaction between the modes leads to an inverse cascade: as energy is transferred to shorter wavelengths a corresponding amount must be transferred to longer wavelength modes to conserve the vorticity. Spectra from the Octupole and from the simulations are peaked at the longest spatial wavelengths.

Boundary conditions also determine the shape of the contours. The highest-energy mode shown in the Octupole spectra is the k = 1 mode. This indicates that the supports are relatively unimportant in determining the

shape of the spectra; however, it appears that the supports are the source of the bump on the spectra in Figs. 8 and 14, and affect mainly the higher modes on the spectra[8].

Montgomery and Joyce[19,20] have examined the statistical mechanics of the 2-D systems and have shown that, if the energy is high enough, the equilibrium solution to the equations of motion consists of two large counterrotating vortices filling the box (this solution corresponds to a negative temperature). In the spectrum for this case, the longest mode has a large fraction of the available energy. Direct comparison of the spectra from the Octupole with simulation results in Ref. 18 is not enough to determine whether the experimental plasmas have a negative temperature in the sense of Ref. 20; however, it is interesting to note that the Octupole contours in Fig. 7 for the collisional plasma show a rough double-vortex pattern that is similar to simulation contours with a negative temperature.

The shape of the spectrum in k-space, in addition to the total amount of vortex energy available, is important in determining the magnitude of the diffusion: the diffusion is dominated by the longest wavelength modes unless $E^2(k)$ increases faster than k^2. The data from the Octupole shows $E^2(k)$ decreasing for increasing k; this means that the first few modes are the most damaging to confinement. A similar result was obtained in a numerical simulation by Okuda and Dawson[9] in which they artificially removed the smallest k-modes and found that diffusion was greatly reduced, even through the energy in those modes was a small fraction of the total energy. Taylor and McNamara[10] also pointed out that the longest wavelength fluctuations are the slowest to disperse.

The macroscopic vortices in Ref. 18 are an equilibrium solution for an inviscid system. The addition of viscosity to this system affects the

process of equilibration. There are two time scales, one for the approach to (inviscid) equilibrium, and the other for the thermalization (which depends on the viscosity and any other dissipative mechanisms which can remove energy from the convective cells). If the first time constant is short, or if the system is close to inviscid-type equilibrium initially, then this type of vortex structure will be observed. This is the case for the Octupole, as the injection process for gun plasmas[5] puts energy initially into long-wavelength modes[8,21]. The vortex modes in the collisional plasma are damped on an ion viscous damping time scale, as shown in the contours in Ref. 5.

VI. CONCLUSIONS

There is a one-to-one correlation between the presence of cells in the Octupole and vortex diffusion: cells are present when the diffusion (calculated from the profile evolution and collector measurements) scales as D_v, and much reduced in amplitude when $D_v \lesssim D_{cl}$. The toroidal spectra have been used to estimate D_v and T* from the potential structure, and the results are in reasonable agreement with the results obtained in the transport studies[5,6]. Since the spectra from the theoretical models are geometry and boundary condition dependent, a detailed comparison between theory and experiment can probably be obtained only in a simpler magnetic field geometry; however, reasonable qualitative agreement was obtained.

The physical model that emerges from the data and the theory is as follows: the initial injection process creates a plasma with a large amount of energy (from charge separation) in turbulent vortex modes. During the first few milliseconds, this initial, non-reproducible distribution evolves into a reproducible structure with the energy concentrated at the longest wavelengths. The spectrum then retains this shape, and decays on a much

longer time scale than the one required to produce the long-wavelength distribution. Diffusion is caused by the vortex modes when the electric fields become uncorrelated. The magnitude of D_v depends on both the magnitude of the electric fields, and the correlation times.

This interpretation also accounts for the enhanced magnitude of D_v obtained in the transport studies over the Okuda-Dawson diffusion coefficient with a thermal spectrum, while preserving the scaling.

ACKNOWLEDGMENTS

Many helpful conversations with Dr. Jerry Navratil are acknowledged, as well as several interesting discussions with Dr. David Montgomery. We would like to extend thanks to Mike Zarnstorff, Jon Twichell, and John Laufenberg for technical support.

This work was supported by a U.S. Department of Energy Contract.

APPENDIX

DIFFERENTIAL OPERATORS IN OCTUPOLE COORDINATES

$$ds_\psi = \frac{d\psi}{2\pi RB}$$

$$ds_\theta = Rd\theta$$

$$ds_\chi = \frac{d\chi}{B}$$

$$\nabla^2\phi = \nabla\cdot\nabla\phi = (2\pi B)^2 \frac{\partial}{\partial\psi} R^2 \frac{\partial\phi}{\partial\psi} + \frac{1}{R^2}\frac{\partial^2\phi}{\partial\theta^2} + B^2\frac{\partial^2\phi}{\partial\chi^2}$$

Using the toroidal eigenmodes $e^{ik\theta}$, we can express ϕ, E_θ, and v_ψ, as

$$\phi(\theta) = \sum_k \phi(k) e^{ik\theta}$$

$$E_\theta(k) = -\frac{ik}{R}\phi(k)$$

$$v_\psi(k) = -\frac{ik}{RB}\phi(k)$$

The density gradient is

$$\vec{\nabla} n = \hat{\psi} 2\pi RB \frac{\partial n}{\partial\psi} + \frac{\hat{\theta}}{R}\frac{\partial n}{\partial\theta} + \hat{\chi} B \frac{\partial n}{\partial\chi}$$

For a purely poloidal field in the Octupole the density is a function only of ψ, and the gradient reduces to the first term.

REFERENCES

[1]W.L. Harries, Phys. Fl. 13(1), 140 (1970); 13(7), 1751 (1970).

[2]A.N. Dellis, J.H.P.C. Megaw, R. Prentice, C.D. King, Plasma Physics and Controlled Nuclear Fusion Research, Proc. 4th International Conference - Madison 1, I.A.E.A., Vienna, p 85.

[3]David Mosher and Francis F. Chen, Phys. Fl. 13(5), 1328 (1970).

[4]Gerald O. Barney and J.C. Sprott, Phys. Fl. 12 (3), 707 (1969).

[5]G.A. Navratil, R.S. Post, and A. Butcher Ehrhardt, Phys. Fl. 20(1), 156. (Jan. 1977).

[6]J.R. Drake, J.R. Greenwood, G.A. Navratil, R.S. Post, Phys. Fl. 20(1), 148 (Jan. 1977).

[7]J.B. Taylor, Phys. Letter 40A(1), 1 (1972).

[8]Alicia Butcher Ehrhardt, U. Wisconsin Ph.D. Thesis (1978).

[9]Hideo Okuda and John M. Dawson, Phys. Fl. 16 (3), 408 (March 1973).

[10]J.B. Taylor and B. McNamara, Phys. Fl. 14 (7), 1492 (1971).

[11]A.B. Ehrhardt, U. Wisconsin PLP 703 (Nov. 1976).

[12]J.R. Drake, U. Wisconsin Ph. D. Thesis, PLP 549, (1974).

[13]A.J. Cavallo, U. Wisconsin Ph. D. Thesis, PLP 628 (1975).

[14]J.R. Greenwood, U. Wisconsin Ph. D. Thesis, PLP 658 (1975).

[15]J. Rudmin, U. Wisconsin Ph. D. Thesis, PLP 587 (1974).

[16]G.A. Navratil, U. Wisconsin PLP 629.

[17]G.A. Navratil, U. Wisconsin Ph. D. Thesis (1976).

FIGURE CAPTIONS

Fig. 1. Cross section of the Octupole showing the movable cart probe and the access to the flux surfaces.

Fig. 2. The floating potential spectrum for 2 msec., 10 msec., and 20 msec. after injection. The data is for a collisional He plasma, supported rings, in the private flux of the lower outer ring. $B_{p\ ave}$= 600G.

Fig. 3. The floating potential spectrum $\phi(k)$ as in Fig. 2., but for $B_{p\ ave}$=100G.

Fig. 4. The calculated vortex diffusion coefficient D_v using data from Fig. 3. ($B_{p\ ave}$= 100G).

Fig. 5. The calculated vortex diffusion coefficient D_v using data from Fig. 2. ($B_{p\ ave}$= 600G).

Fig. 6. The total energy $\Sigma\phi^2(k)$ as a function of time using data from Figs. 2. and 3. (collisional He plasma).

Fig. 7. Floating potential contours in the ψ-θ plane at several times after injection. Collisional He plasma, supported rings. Data taken in the private flux of the lower inner ring; $B_{p\ ave}$= 480G.

Fig. 8. $E^2(k)$ vs. k at 3 msec. after injection of a collisional He plasma, for various flux surfaces. Data taken in the private flux of the lower inner ring (supported) with $B_{p\ ave}$= 480G.

Fig. 9. Same as Fig. 8. but 7 msec. after injection.

Fig. 10. $\Sigma E_\theta{}^2(k)$ vs. ψ for several times after injection. Data measured for a He plasma in the private flux of the lower outer ring. $B_{p\ ave}$= 100G.

Fig. 11. Spatial and temporal dependence of D_v for a collisional He plasma. Data taken in the private flux of the lower ring. $B_{p\ ave}$= 480G.

Fig. 12. Floating potential contours in the ψ-θ plane for several times after injection. The plasma is a collisionless H plasma. Data taken in the private flux of the lower ring (supported). The ring supports (levators) are indicated as OL (outer levator) and IL (inner levator).

Fig. 13. The spectrum $E^2(k)$ for the collisionless H plasma for several times after injection. Data taken in the private flux, lower outer ring, supported. $B_{p\ ave} = 2kG$, $\psi = 4.09$.

Fig. 14. Same as Fig. 13. but for $\psi = 4.5$.

Fig. 15. The calculated diffusion coefficient vs. time for the data of Figs. 13. and 14.

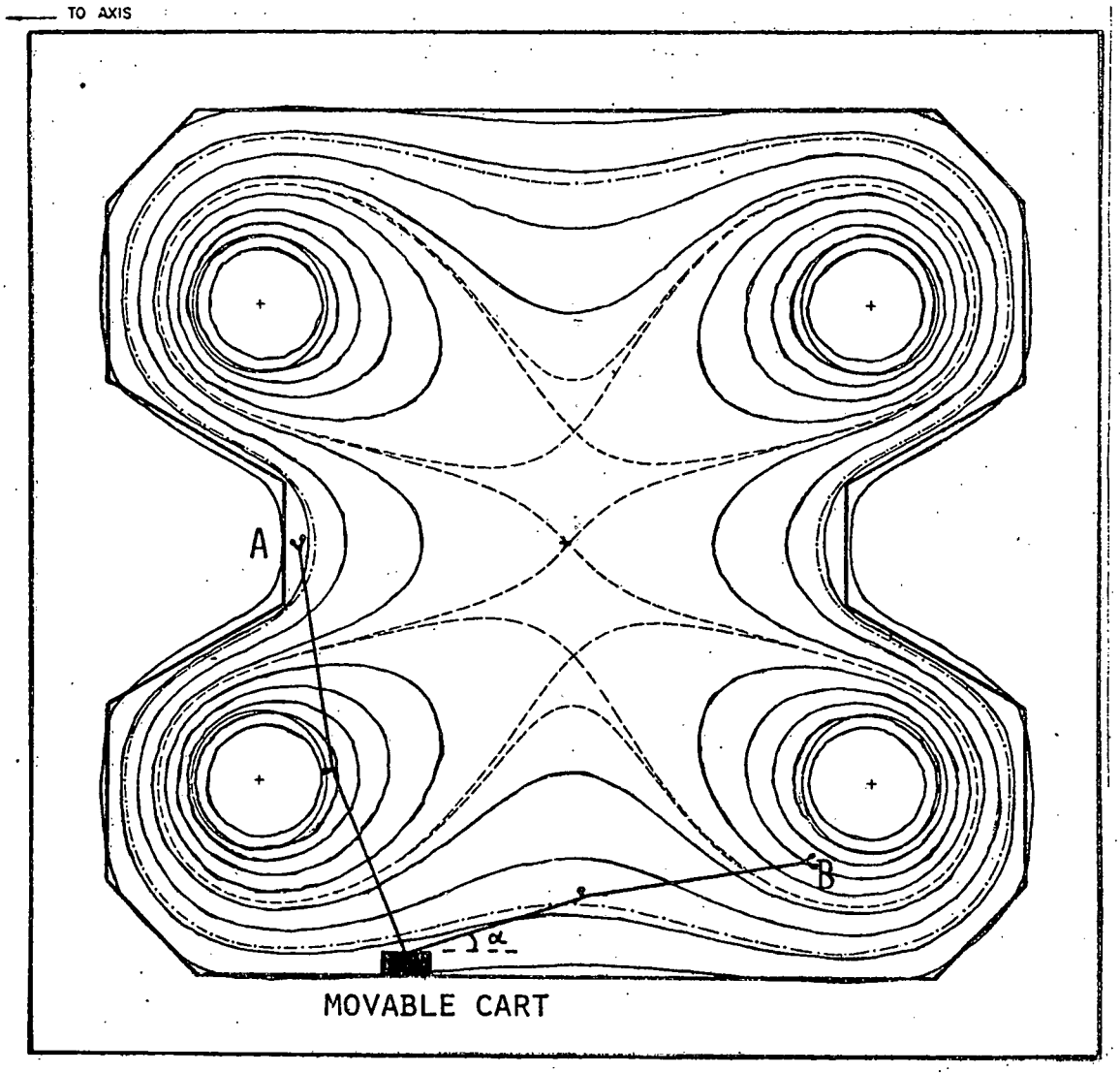

FIGURE 1

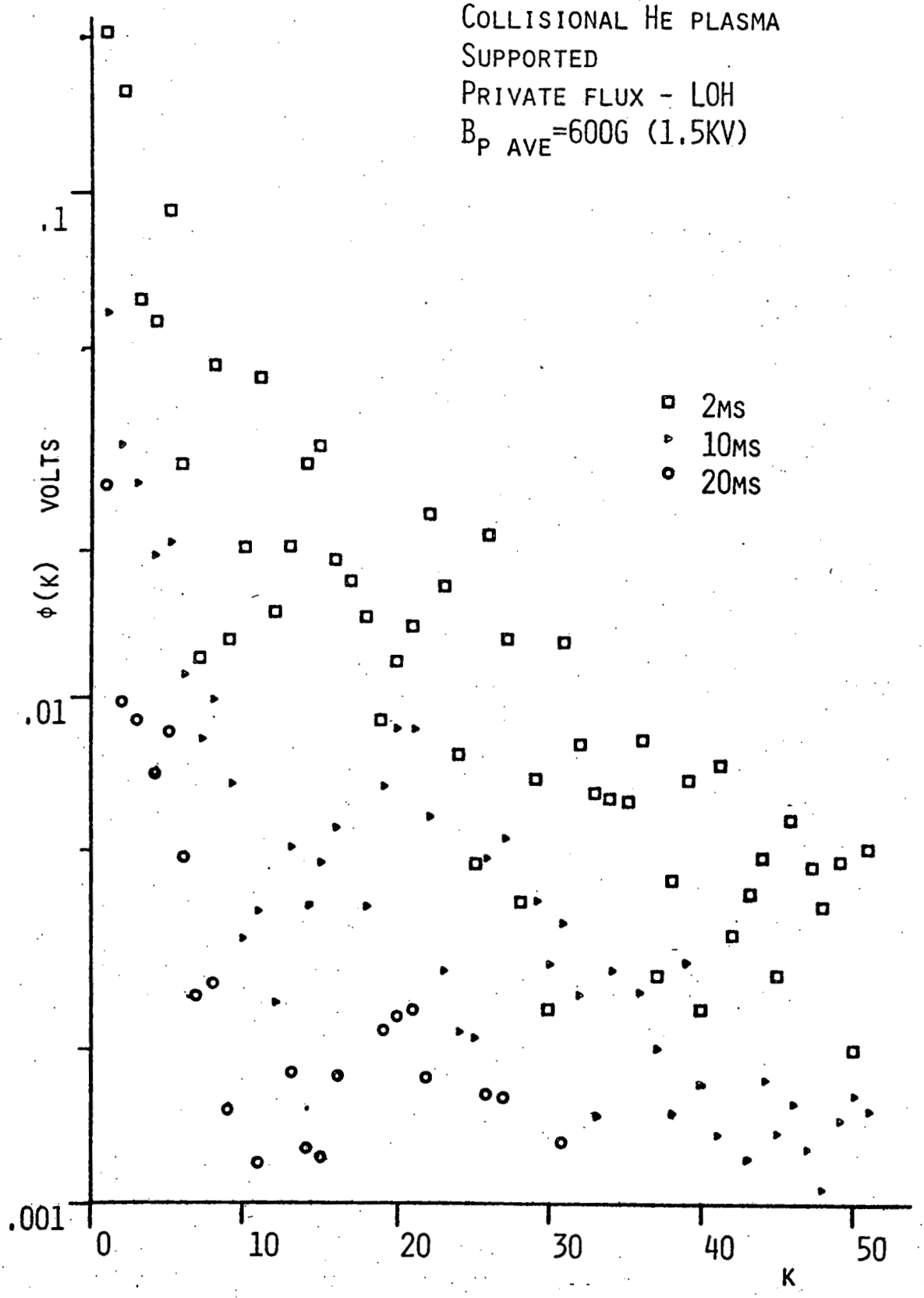
COLLISIONAL HE PLASMA
SUPPORTED
PRIVATE FLUX - LOH
$B_{P\ AVE}$=600G (1.5KV)
2MS
10MS
20MS
.1
.01
.001
φ(K) VOLTS
0
10
20
30
40
50
K

FIGURE 2

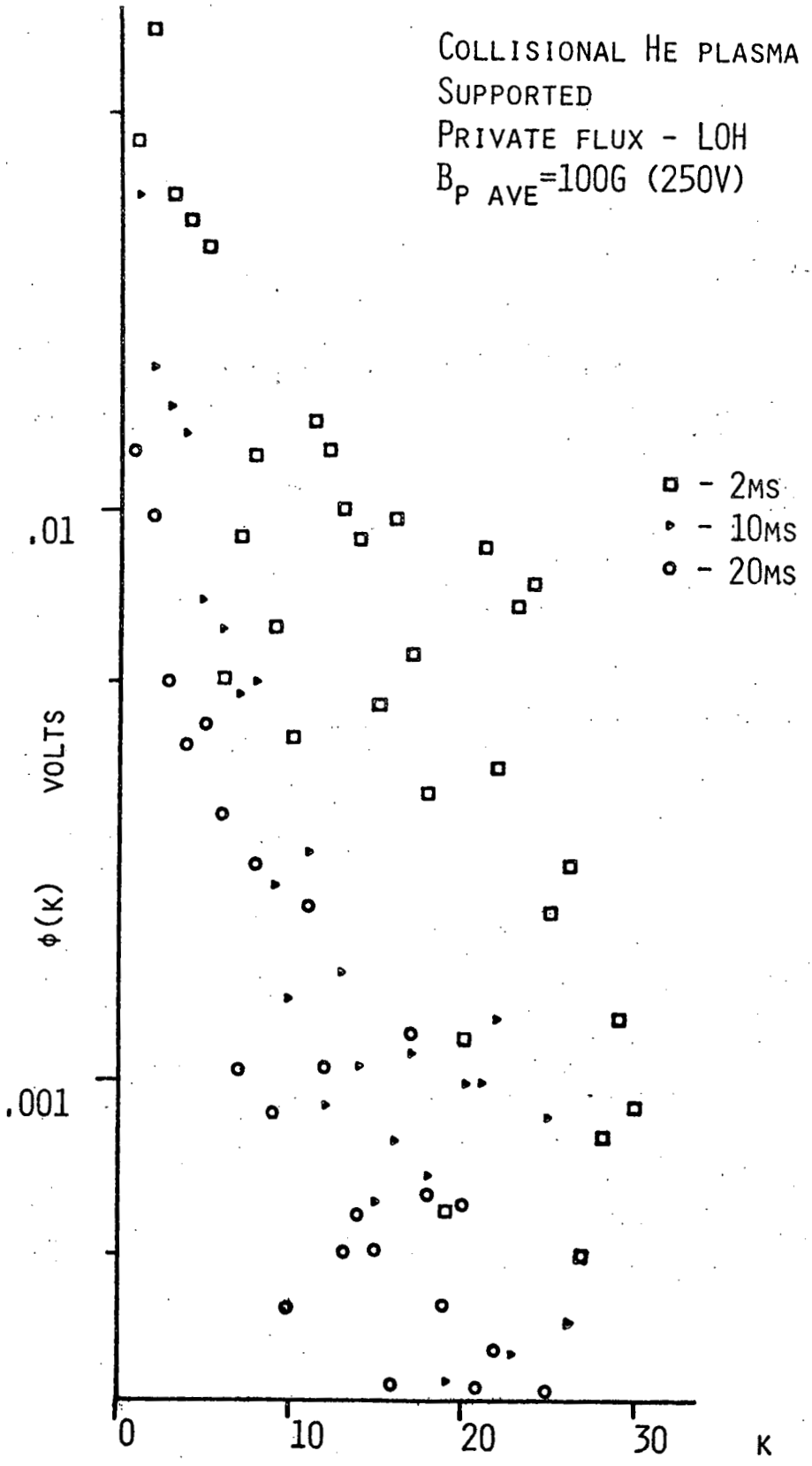
COLLISIONAL HE PLASMA
SUPPORTED
PRIVATE FLUX - LOH
$B_{P\ AVE}$=100G (250V)
□ - 2MS
▸ - 10MS
○ - 20MS
.01
.001
φ(K) VOLTS
0
10
20
30
K

FIGURE 3

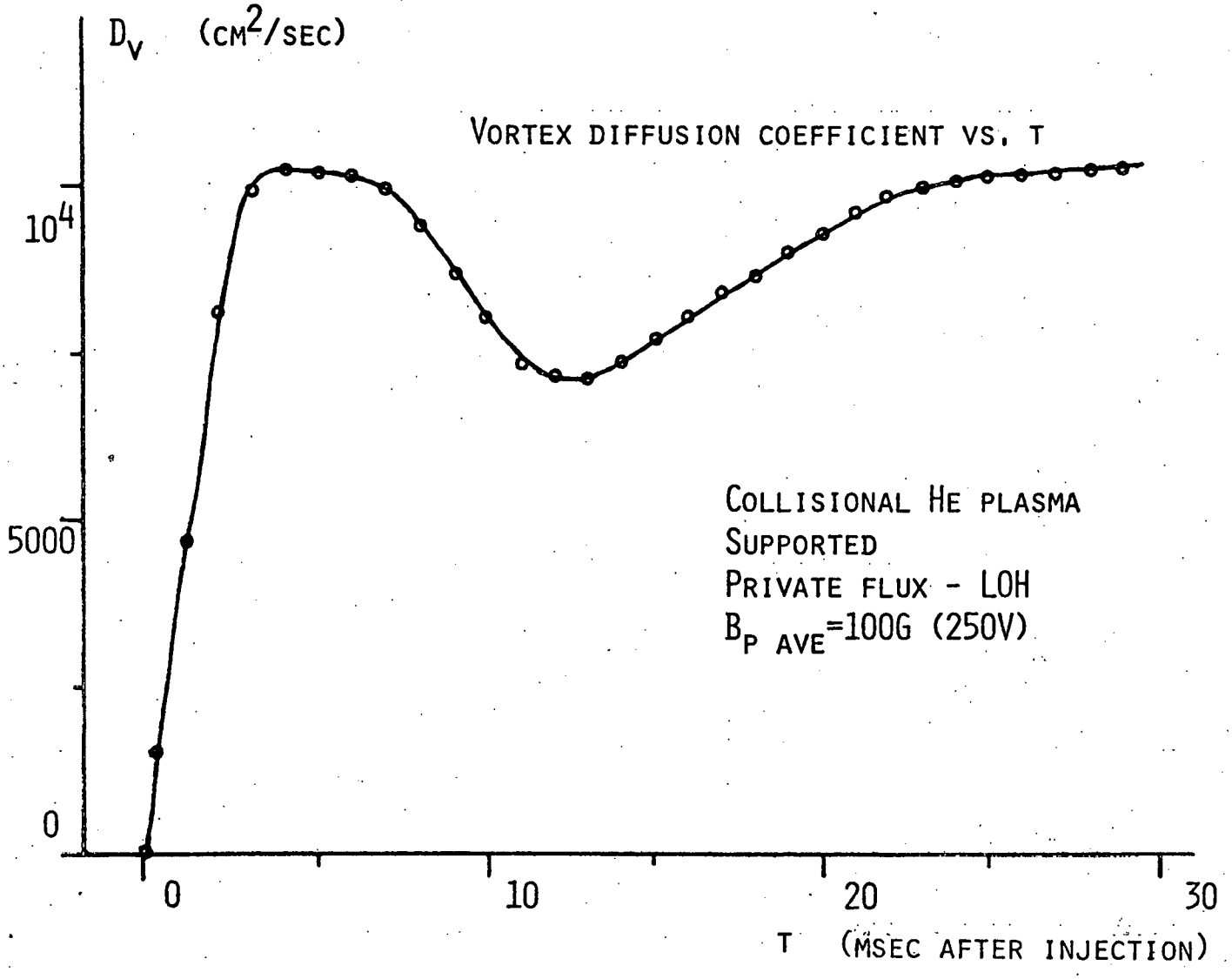
D_V (CM^2/SEC)
VORTEX DIFFUSION COEFFICIENT VS. T
10^4
5000
0
0
10
20
30
T (MSEC AFTER INJECTION)
COLLISIONAL HE PLASMA
SUPPORTED
PRIVATE FLUX - LOH
$B_{P\ AVE}$=100G (250V)

FIGURE 4

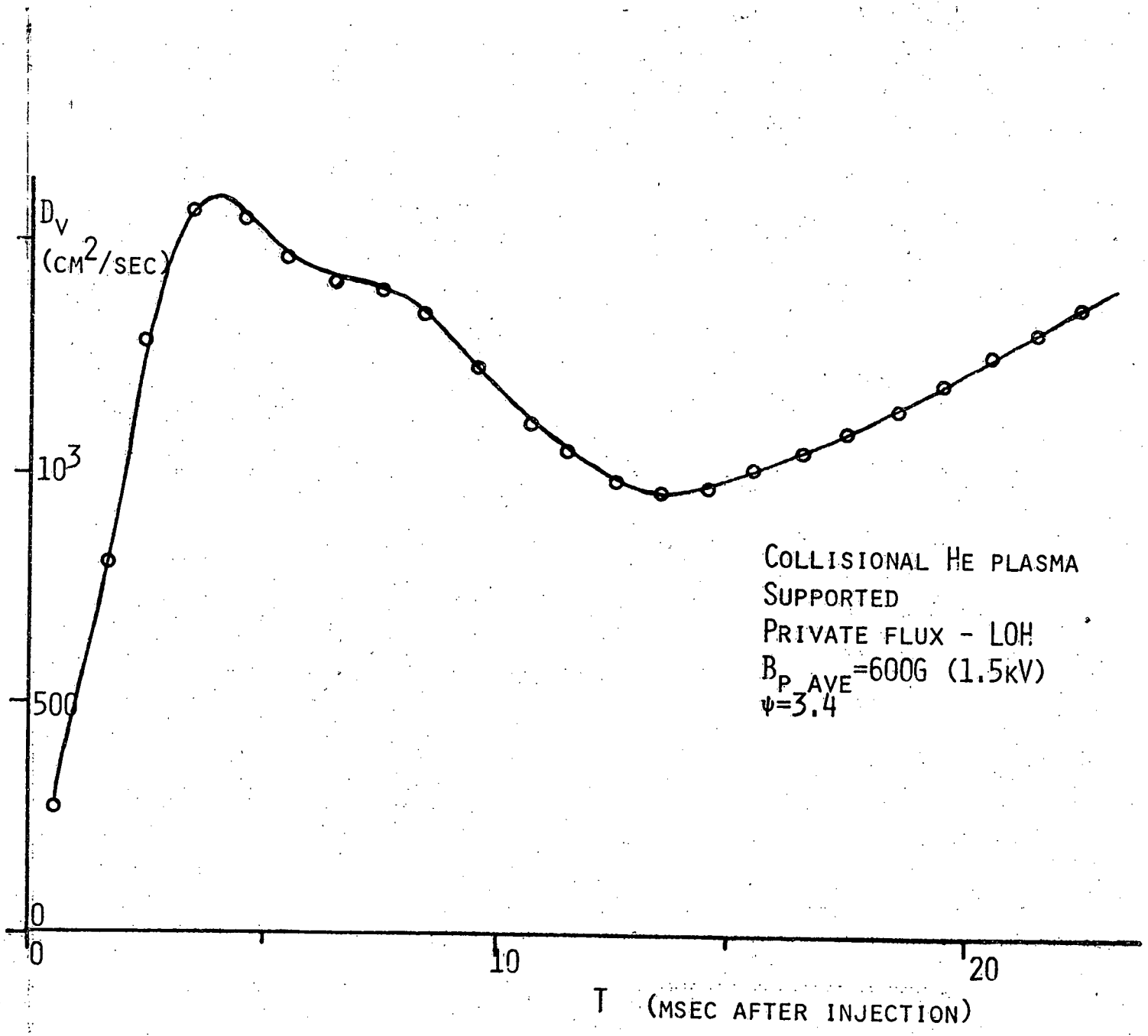
D_V
(CM^2/SEC)
10^3
500
0
0
10
20
T (MSEC AFTER INJECTION)
COLLISIONAL HE PLASMA
SUPPORTED
PRIVATE FLUX - LOH
$B_{P\,AVE}$=600G (1.5KV)
ψ=3.4

FIGURE 5

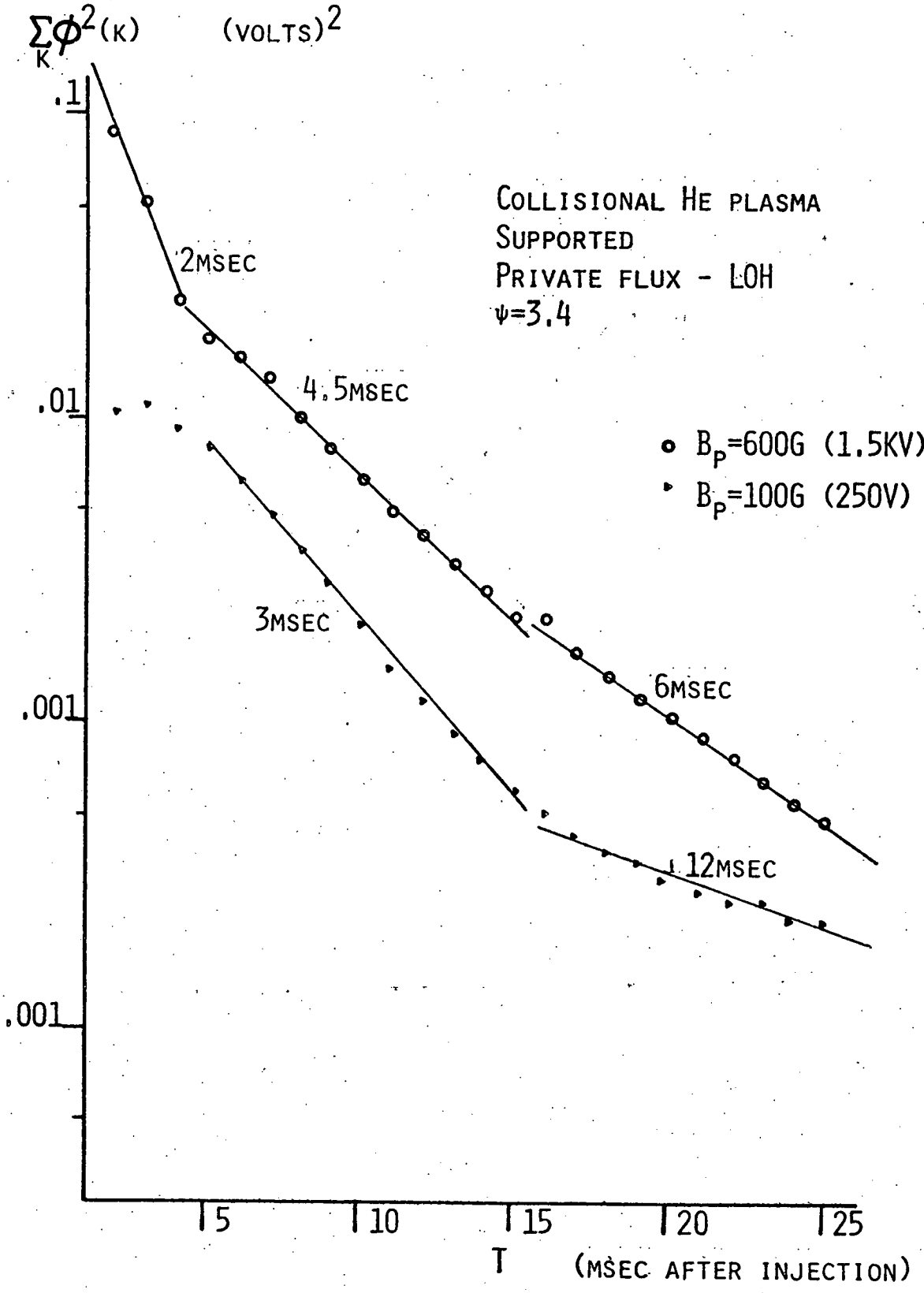
$\sum_K \phi^2(K)$ (VOLTS)^2
.1
.01
.001
.001
2MSEC
4.5MSEC
3MSEC
6MSEC
12MSEC
COLLISIONAL HE PLASMA
SUPPORTED
PRIVATE FLUX - LOH
ψ=3.4
B_p=600G (1.5KV)
B_p=100G (250V)
5
10
15
20
25
T
(MSEC AFTER INJECTION)

FIGURE 6

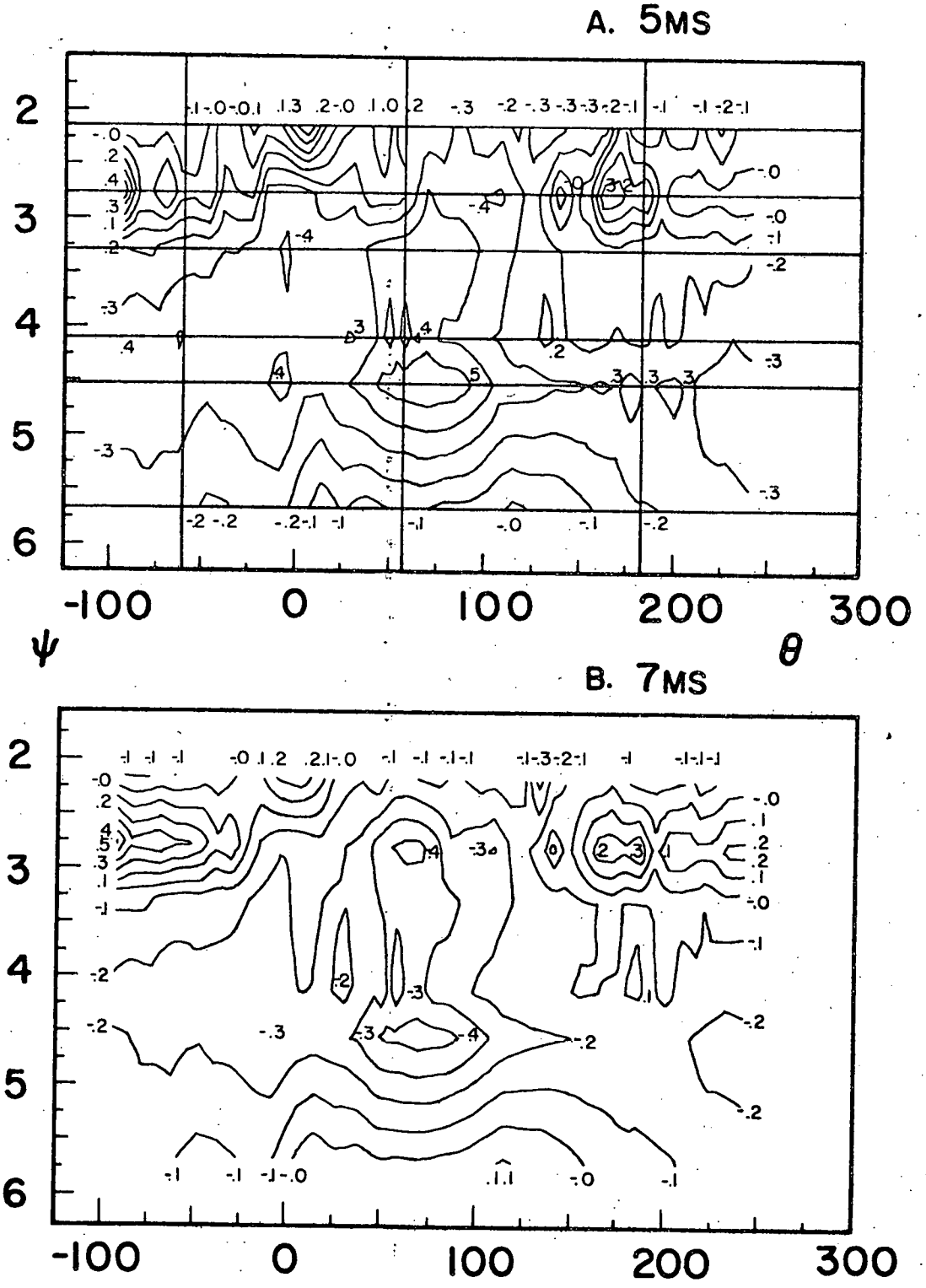

FIGURE 7

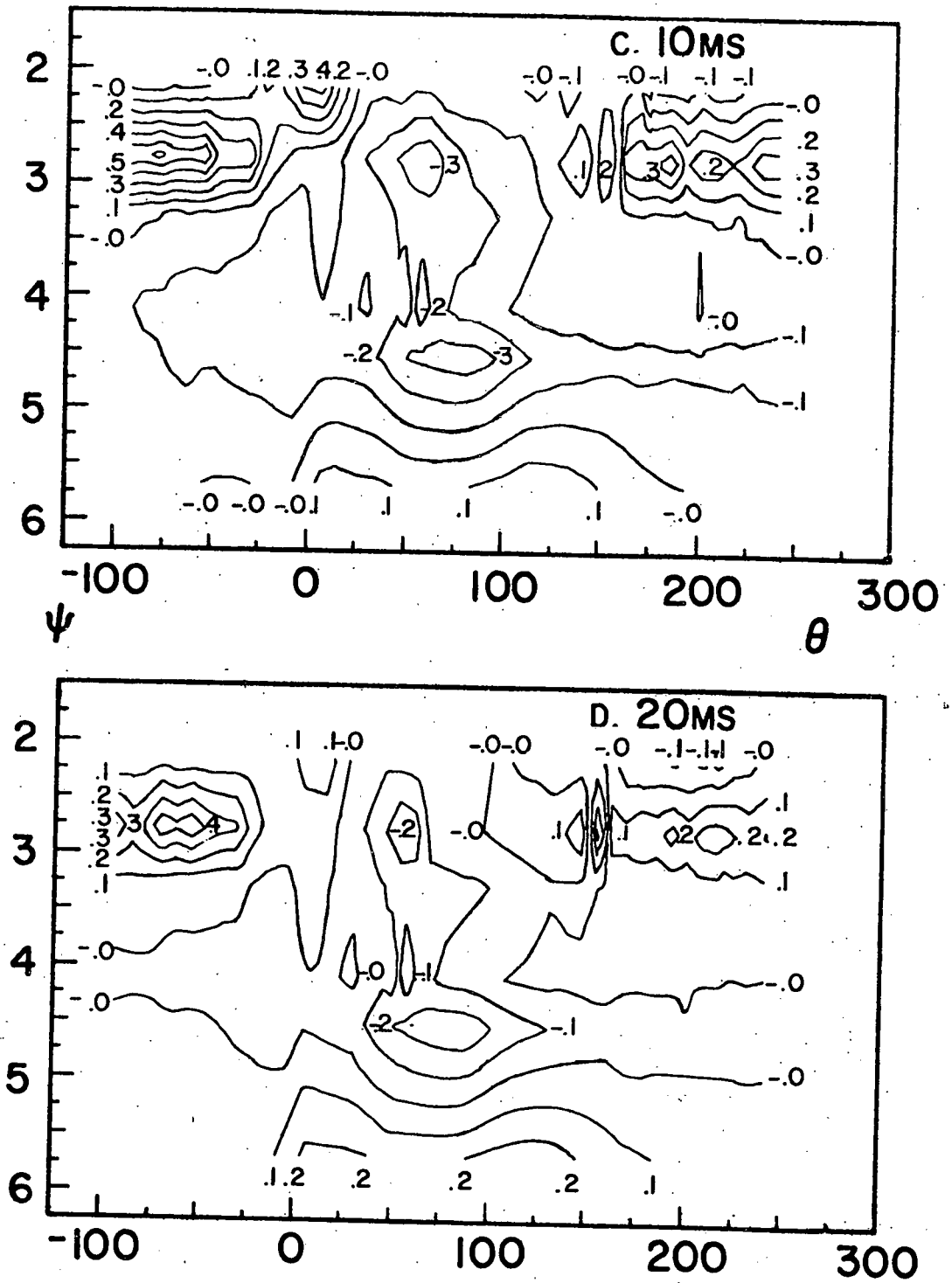

FIGURE 7

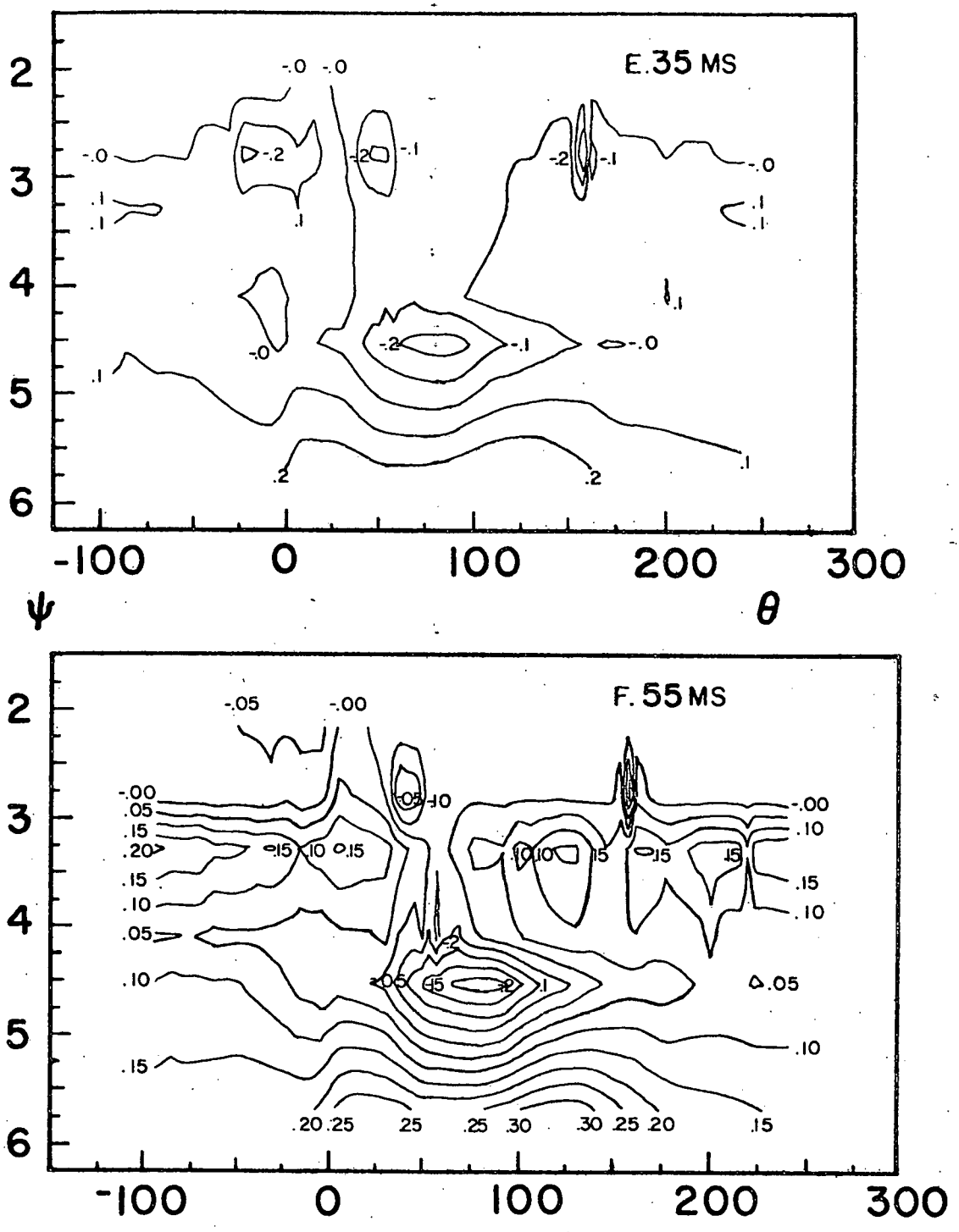

FIGURE 7

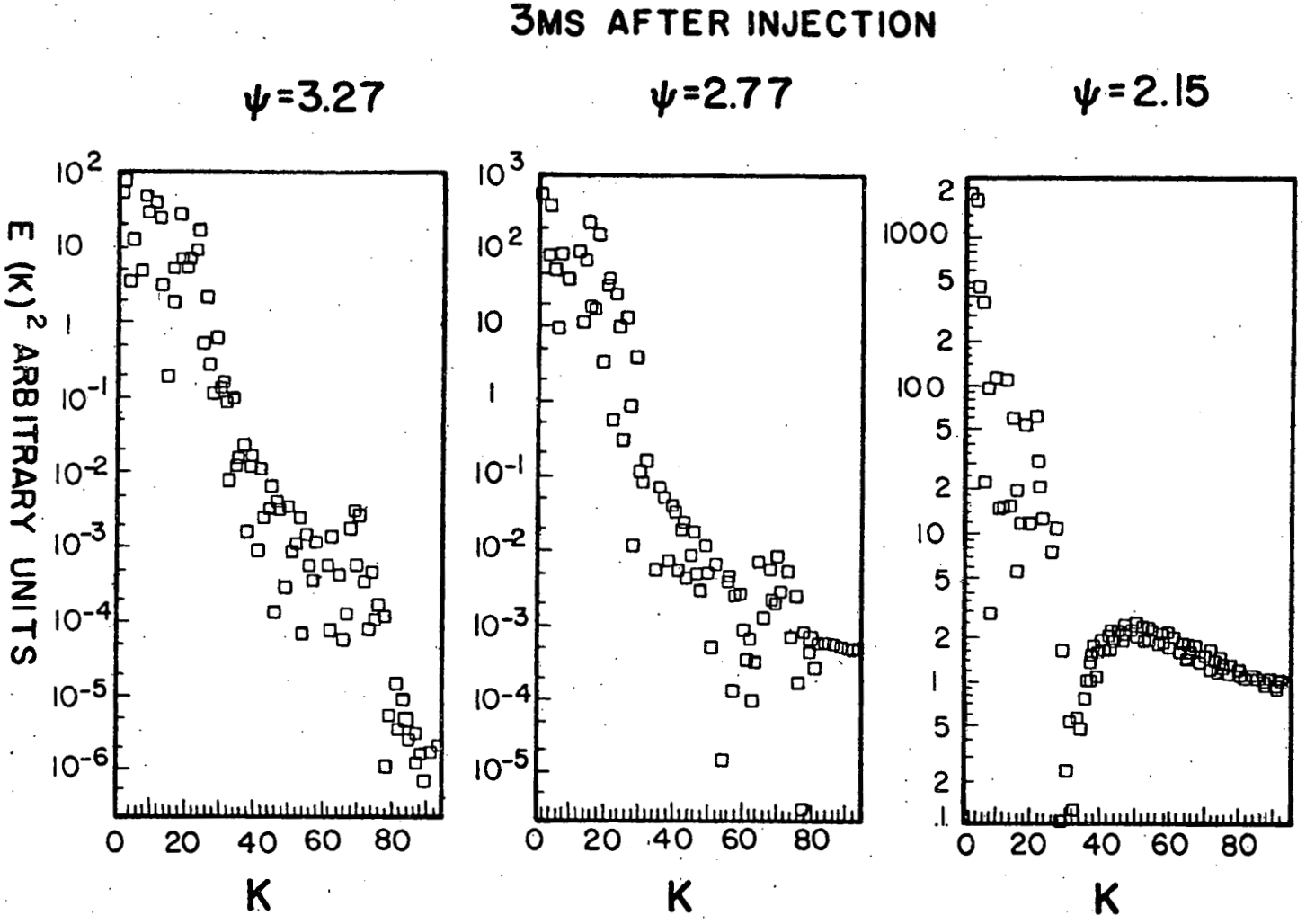

FIGURE 8

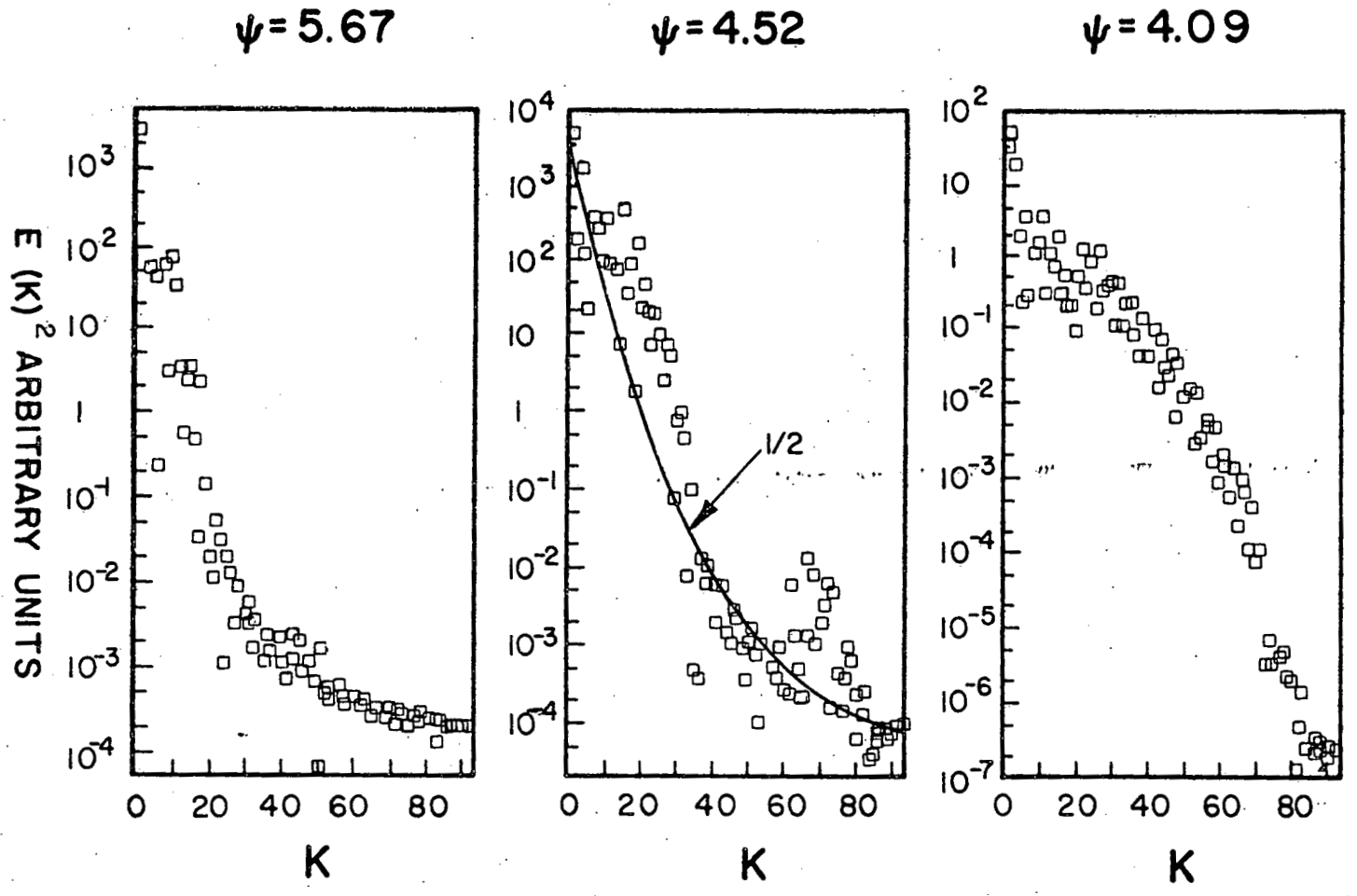
3MS AFTER INJECTION
ψ = 5.67
ψ = 4.52
ψ = 4.09
E (K)² ARBITRARY UNITS
1/2
K
K
K

FIGURE 8

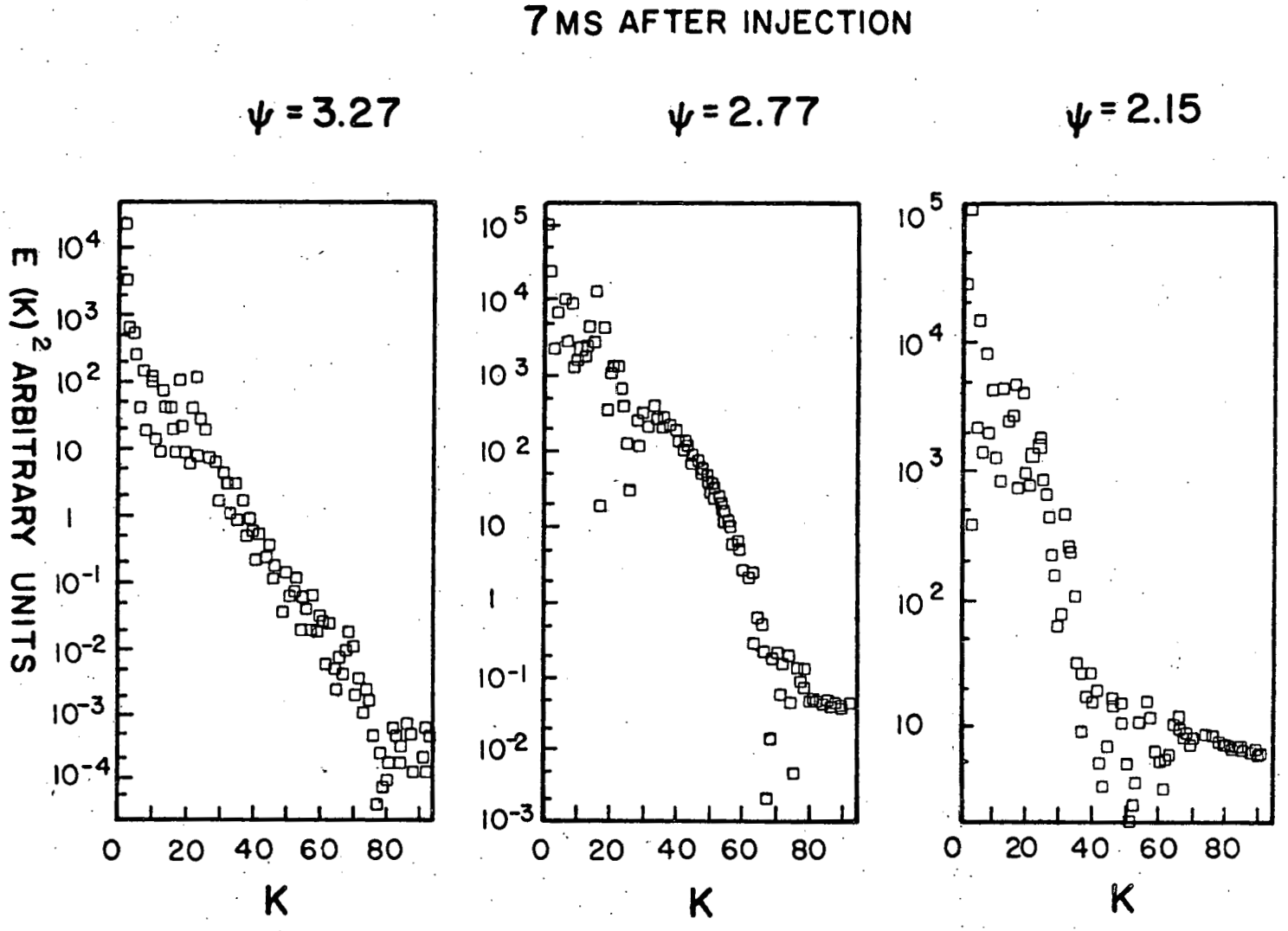

FIGURE 9

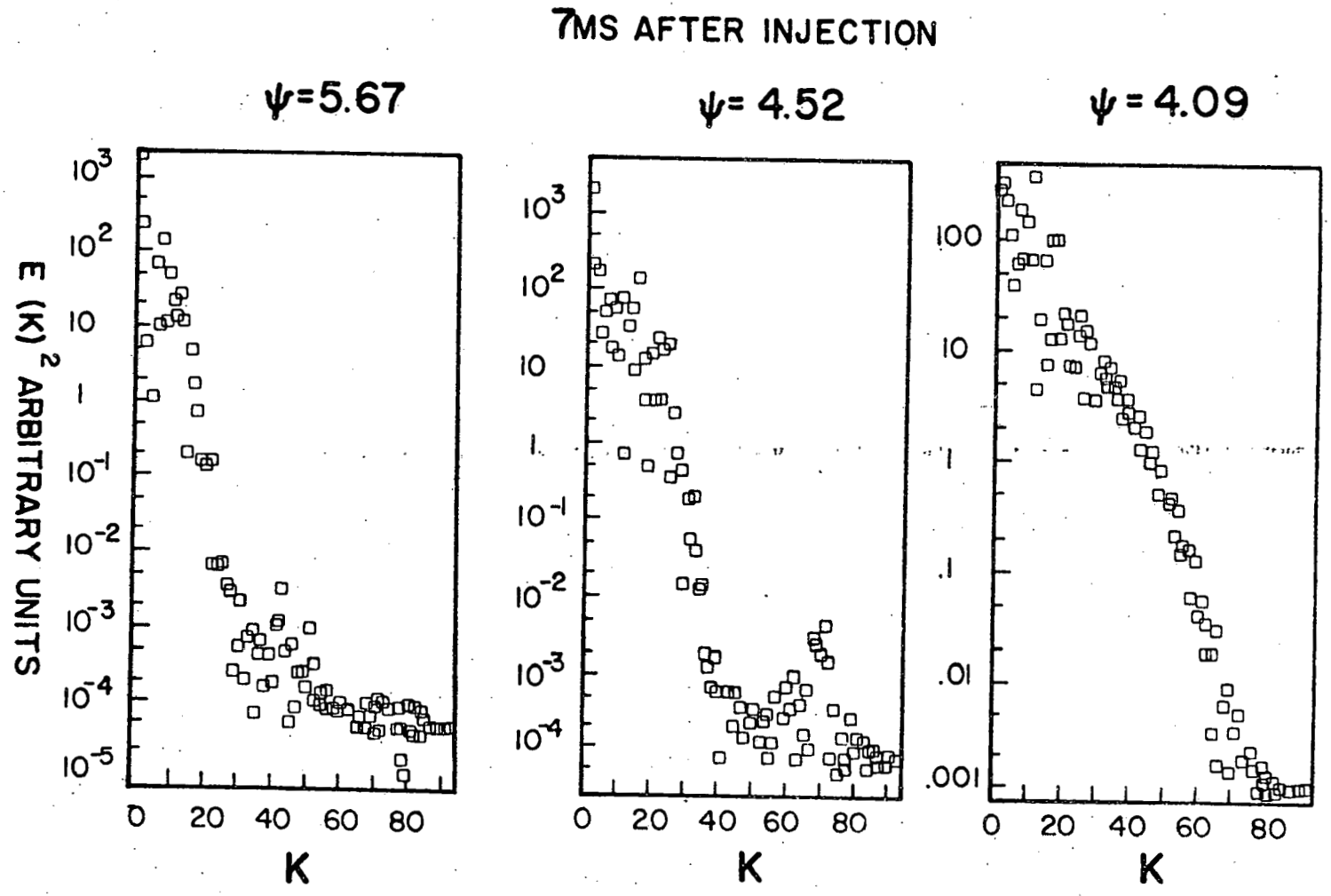

FIGURE 9

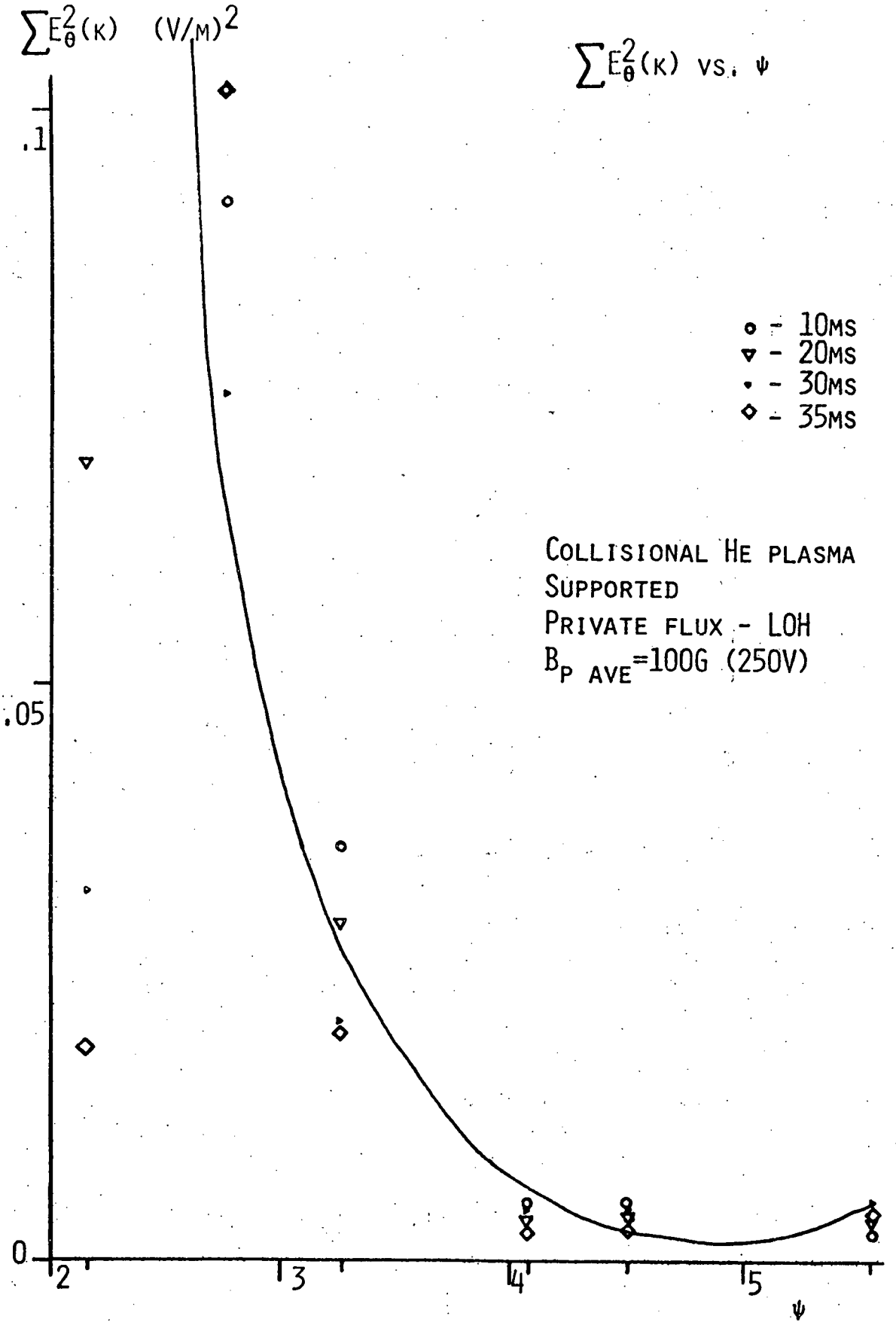
$\sum E_\theta^2(K)$ $(V/M)^2$
$\sum E_\theta^2(K)$ vs. ψ
.1
.05
0
2
3
4
5
ψ
o - 10MS
▽ - 20MS
• - 30MS
◇ - 35MS
COLLISIONAL HE PLASMA
SUPPORTED
PRIVATE FLUX - LOH
$B_{P\ AVE}$=100G (250V)

FIGURE 10

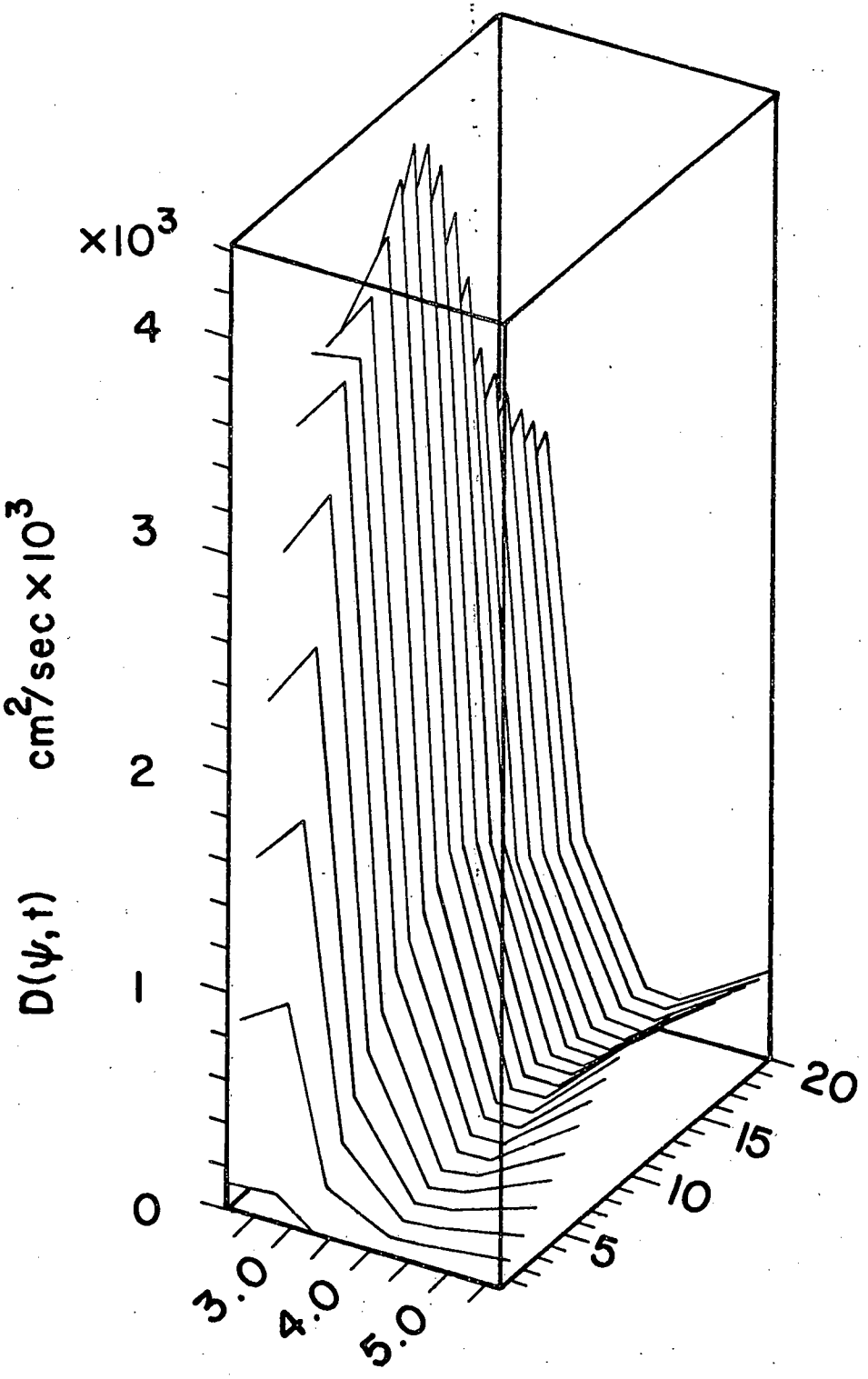

FIGURE 11

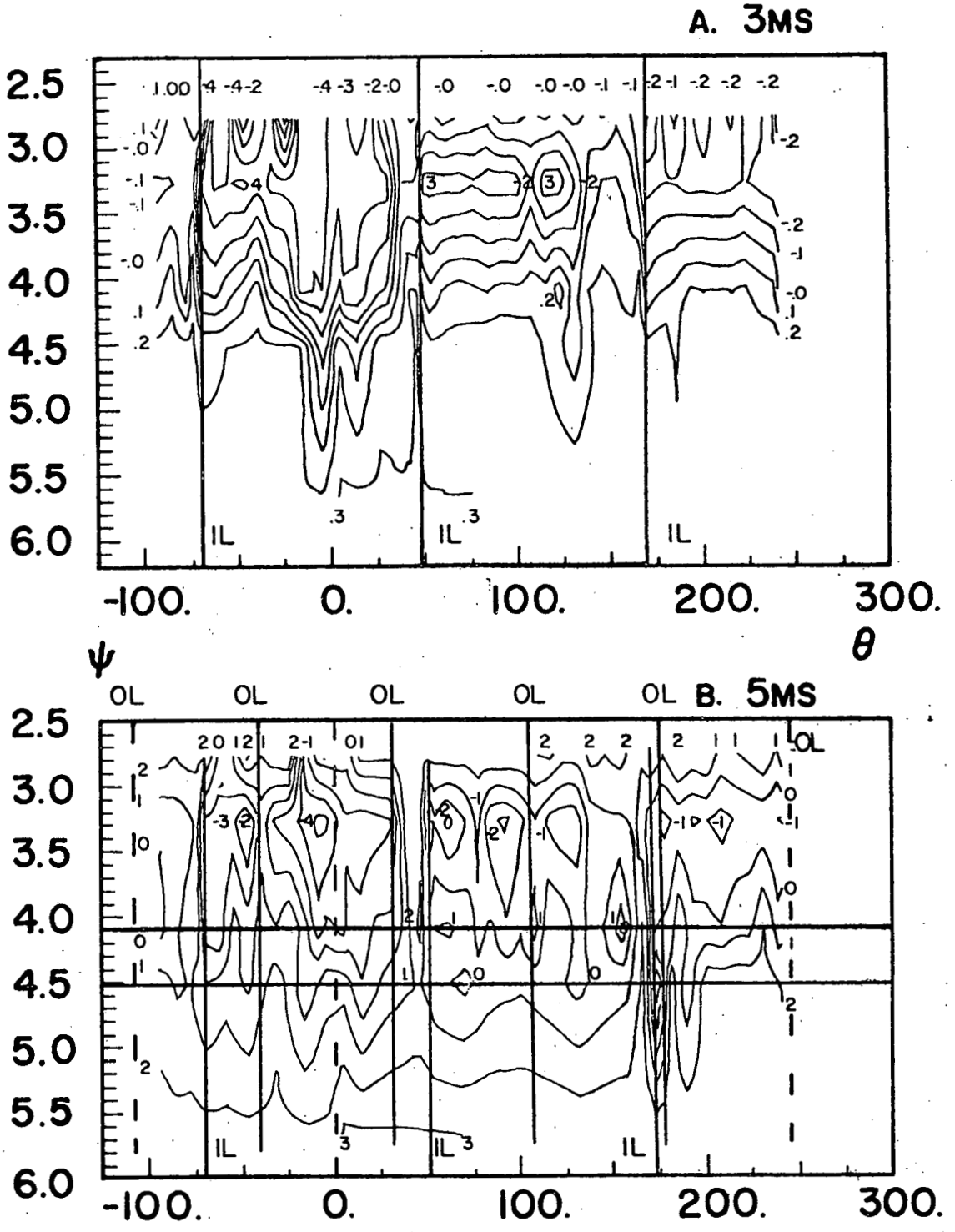

FIGURE 12

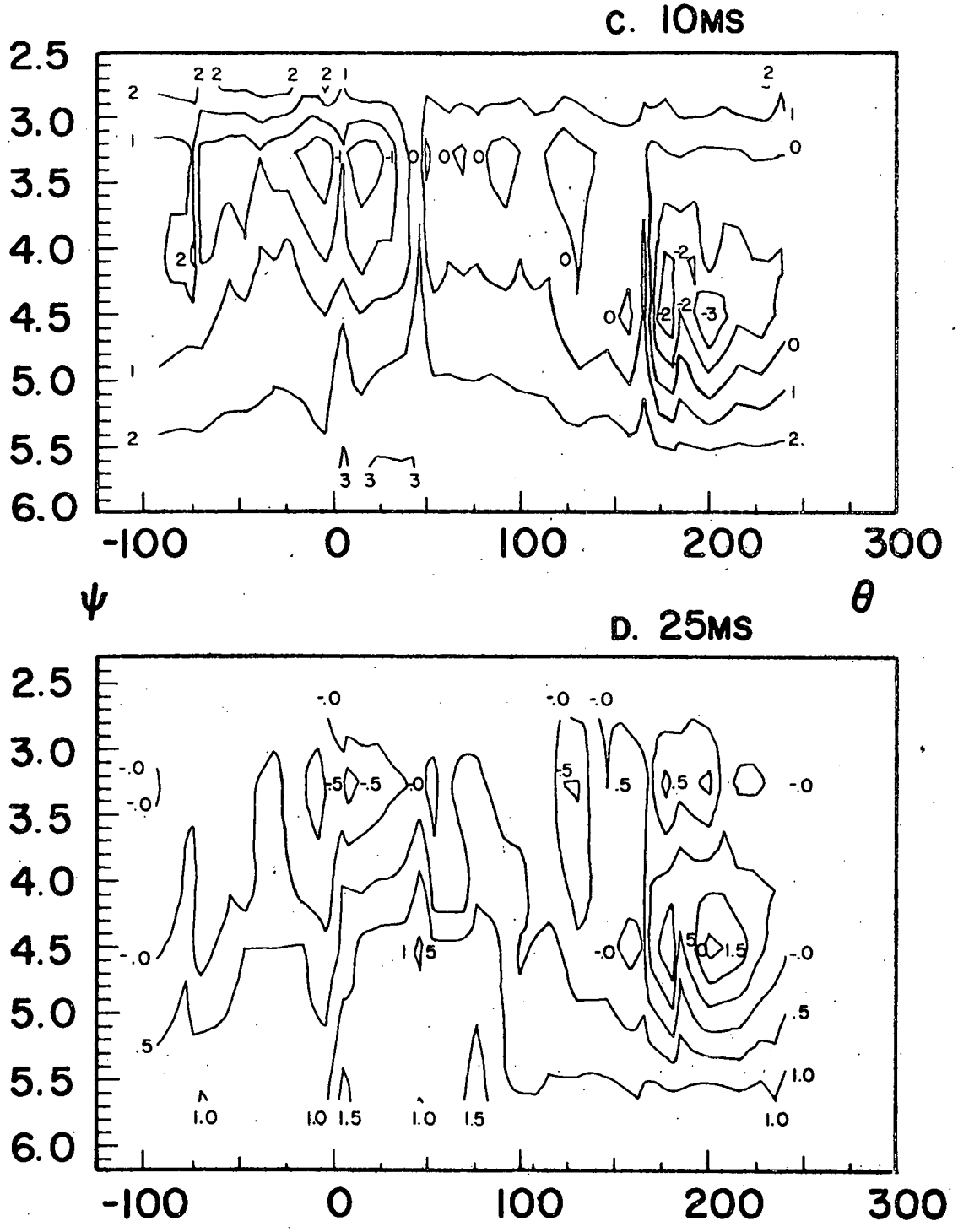
C. 10MS
2.5
3.0
3.5
4.0
4.5
5.0
5.5
6.0
-100
0
100
200
300
ψ
θ
D. 25MS
2.5
3.0
3.5
4.0
4.5
5.0
5.5
6.0
-100
0
100
200
300

FIGURE 12

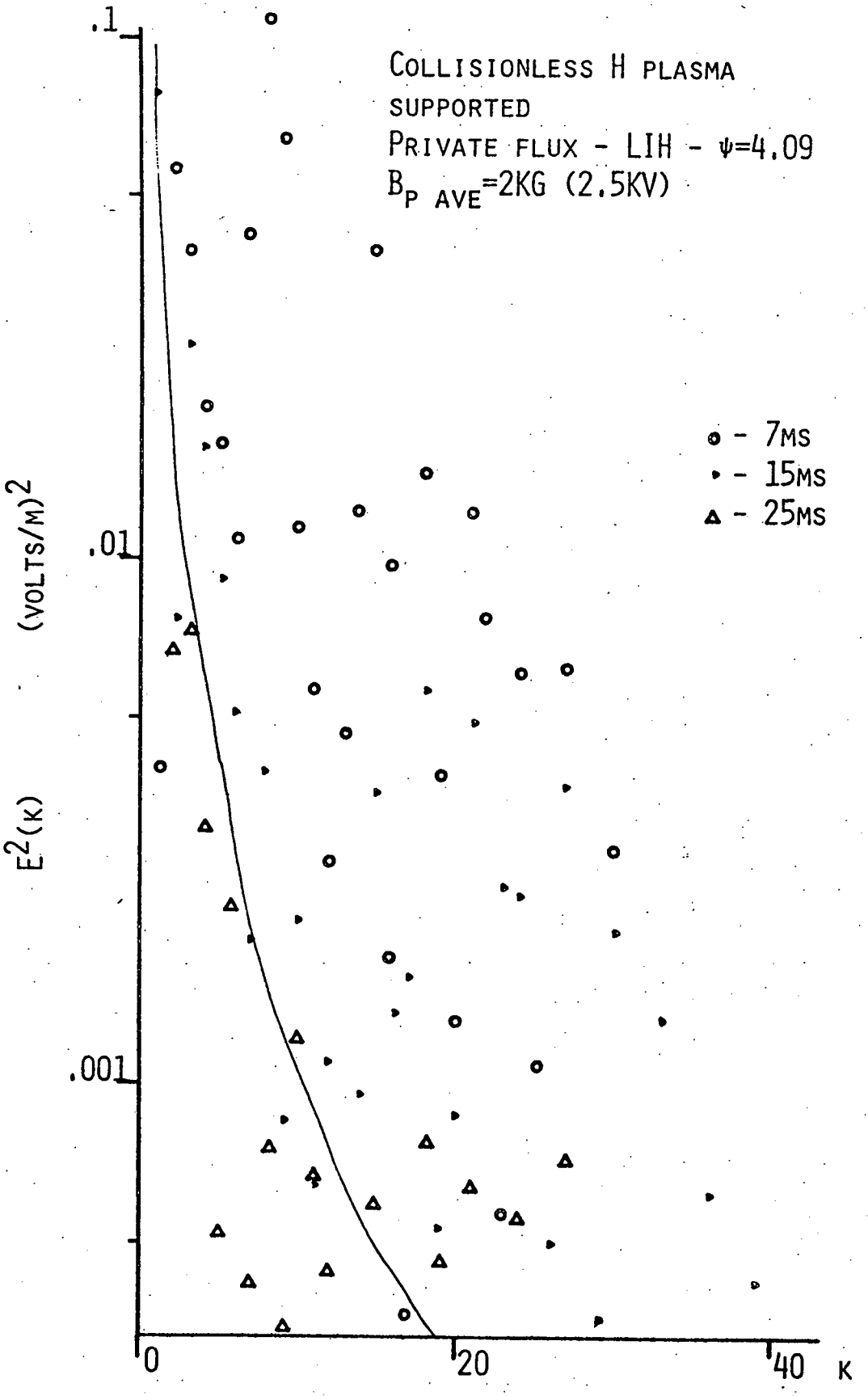
COLLISIONLESS H PLASMA
SUPPORTED
PRIVATE FLUX - LIH - ψ=4.09
$B_{P\ AVE}$=2KG (2.5KV)
o - 7MS
• - 15MS
Δ - 25MS
.1
.01
.001
$E^2(K)$ (VOLTS/M)^2
0
20
40
K

FIGURE 13

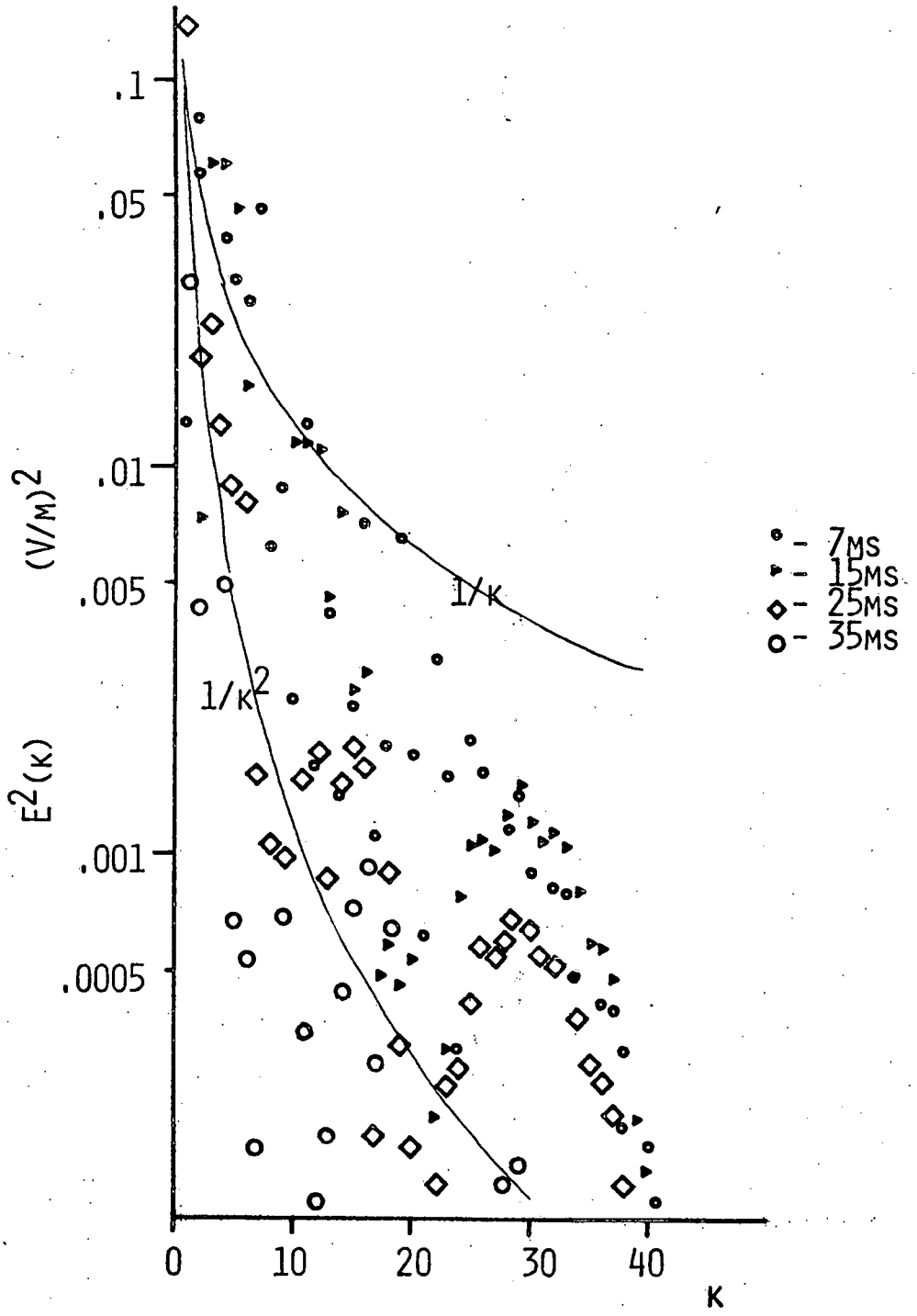
.1
.05
.01
.005
.001
.0005
$E^2(K)$
$(V/M)^2$
1/K
$1/K^2$
0
10
20
30
40
K
7MS
15MS
25MS
35MS

FIGURE 14

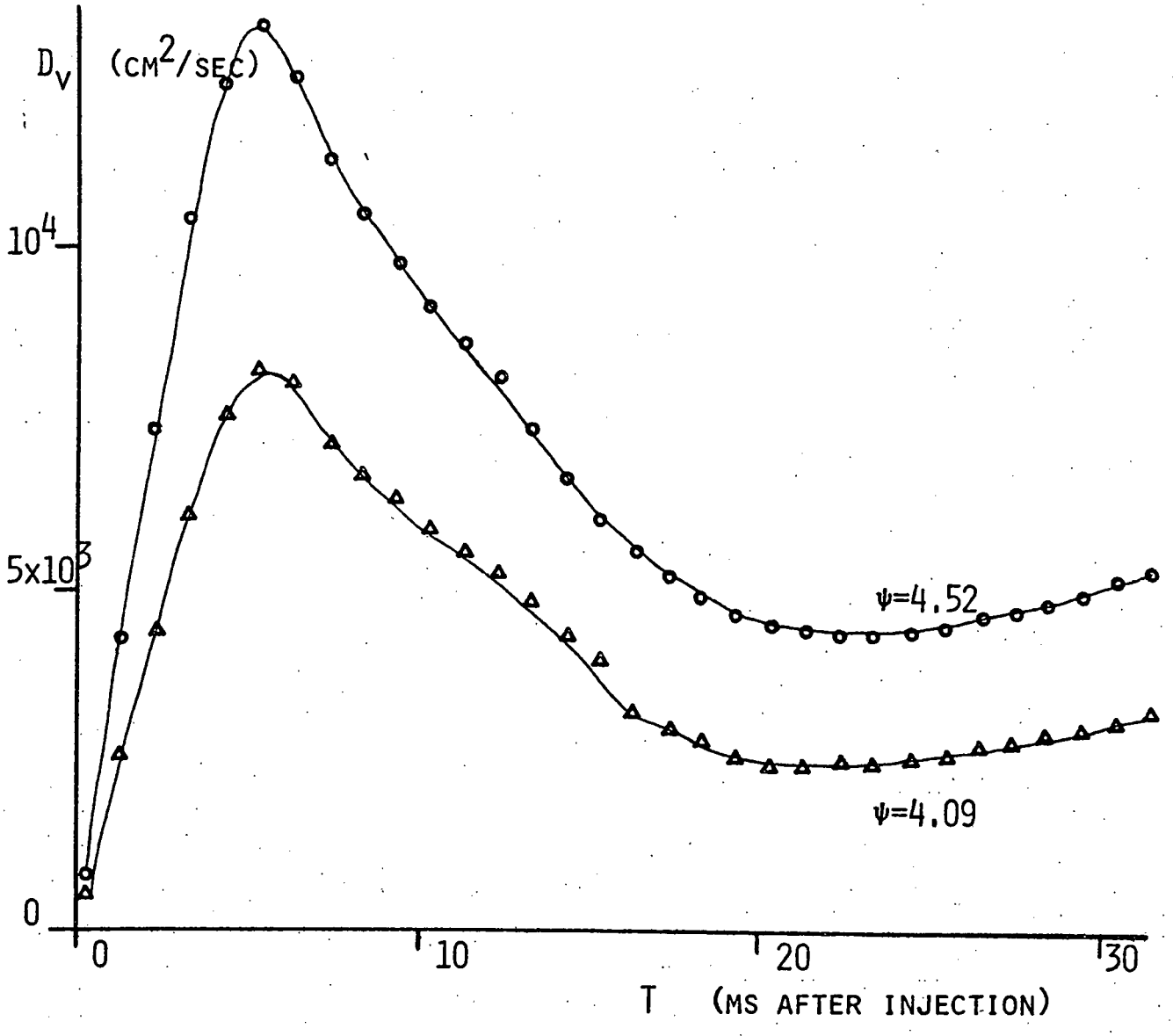

FIGURE 15

EXTERNAL DISTRIBUTION IN ADDITION TO UC-20

R.W. Conn, University of California, Los Angeles
J.W. Flowers, University of Florida
H.S. Robertson, University of Miami, FL
E.G. Harris, University of Tennessee
M. Kristiansen, Texas Technical University
Plasma Research Laboratory, Australian National University
P.E. Vandplas, Association Euratom-Etat Belge, Belgium
P. Sananaka, Institute de Fisica-Unicamp, Brazil
A.M. Dupas, C.E.N.G., Dph-PFG-SIG, France
M.A. Loyau, Centre d'Etudes Nucleaires, France
G. VonGierke, Max-Planck-Institut Für Plasma Physic, Germany
R. Toschi, Associazione Euratom-Cnen Sulla Fusion, Cento Gas Ionizzati, Italy
K. Takayma, IPP Nagoy Imoversotu, Japan
K. Uo, Kyote University, Japan
K. Yamanto, JAERI, Japan
B. Lehnert, Royal Institute of Technology, Sweden
E.S. Weibel, CRPP, Ecole Polytechnique Federale de Lausanne, Switzerland
A. Gibson, Culham Laboratory, UK
R.S. Pease, Culham Laboratory, UK
D.R. Sweetman, Culham Laboratory, UK
J.B. Taylor, Culham Laboratory, UK
M.H. Hellberg, University of Natal, Durban, South Africa
Cheng-chung Yang, Chinese Academy of Sciences, Lanchow, Peoples Republic of China
Chi-shis Li, Chinese Academy of Sciences, Peking, Peoples Republic of China
Hsiao-wu Cheng, Chinese Academy of Sciences, Shanghai, Peoples Republic of China
Yi-chung Cho, Chinese Academy of Sciences, Peking, Peoples Republic of China
Fu-chia Yang, Futan University, Peoples Republic of China
Mei-ling Yeh, Chinese Academy of Sciences, Lanchow, Peoples Republic of China
Wei-chung Change, Chinese Academy of Sciences, Shanghai, Peoples Republic of China
Kuei-wu Wang, Chinese Academy of Sciences, Loshan County, Peoples Republic of China
Chun-hsien Chen, Chinese Academy of Sciences, Peking, Peoples Republic of China
Li-tsien Chiu, Chinese Academy of Sciences, Peking, Peoples Republic of China
Miao-sun Chen, Chinese Academy of Sciences, Peking, Peoples Republic of China

6 for Chicago Operations Office
10 for individuals in Washington Offices

INTERNAL DISTRIBUTION IN ADDITION TO UC-20

100 for local group and file